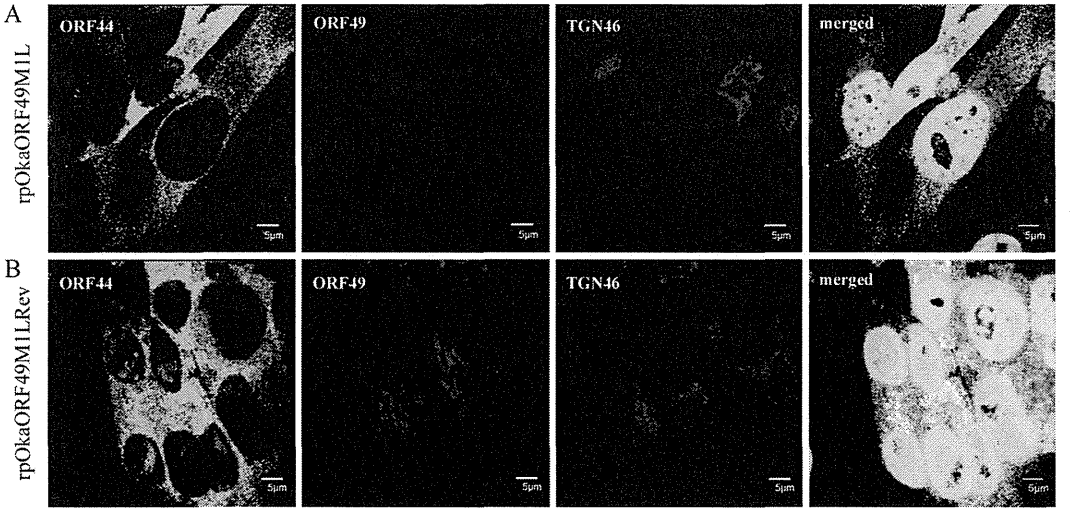

FIG 7 Localization of ORF44p and ORF49p in rpOkaORF49M1L-infected MeWo cells. rpOkaORF49M1L-infected (A) and rpOkaORF49M1LRev-infected (B) MeWo cells were fixed at 48 hpi and triple labeled for ORF44p (green), ORF49p (red), and TGN46 (blue). Nuclei were stained with Hoechst 33342 (cyan). Scale bars, 5 μm.

The phenylalanine at amino acid position 129 of ORF44p functions in the conserved interaction and is essential for VZV infection. In the process of ORF44 cloning, one mutant showed a T-to-C substitution at nt 385, which led to a phenylalanine-to-serine transition at aa 129 (F129S). In cells coexpressing ORF44F129Sp and ORF49p, ORF44F129Sp did not accumulate on the TGN and was not coimmunoprecipitated with ORF49p (data not shown).

To examine whether 129F functions specifically in the conserved interaction in VZV, alanine scanning was performed around 129F (Fig. 1B). ORF44T128Ap, ORF44F129Ap, and ORF44K130Ap showed similar distributions, and none of these mutants localized to the TGN when expressed alone (data not shown), as observed in cells expressing ORF44p alone (Fig. 5A). Coexpression of ORF44T128Ap and ORF44K130Ap with ORF49p (Fig. 8A and C, respectively) resulted in their colocalization with ORF49p at the TGN, as observed in cells coexpressing ORF44p and ORF49p (Fig. 5C). In contrast, ORF44F129Ap was dispersed throughout the cytoplasm and failed to accumulate on the TGN, even when coexpressed with ORF49p (Fig. 8B). The levels of expression of ORF44T128Ap, ORF44F129Ap, and ORF44K130Ap were almost equal (Fig. 6A, lanes 2, 3, and 4, respectively), and ORF44T128Ap and ORF44K130Ap were coimmunoprecipitated with ORF49p (Fig. 6B, lanes 2 and 4, respectively), whereas ORF44F129Ap was not coimmunoprecipitated with ORF49p (Fig. 6B, lane 3).

The results for F129S and F129A suggest that the binding site for ORF49p might reside in an N-terminal domain, as was recently reported for the pUL16 of HSV-1 (26). Therefore, stop codons were inserted at positions to either side of codon 129F (i.e., at I121stop and P136stop). In addition, a construct containing both the F129A and P136stop mutations was made (Fig. 1B). All three mutants were expressed at their predicted size (Fig. 6A, lanes 8, 9, and 10), and only the ORF44P136stop protein was coimmunoprecipitated with ORF49p (Fig. 6B, lane 9), whereas the ORF44I121stop and ORF44F129AP136stop proteins were not (Fig. 6B, lanes 8 and 10, respectively). Consistent with this, only the ORF44P136stop protein accumulated on the TGN with ORF49p (Fig. 8E), and the other two mutants did not (Fig. 8D and F), despite the diffused cytoplasmic localization of all mutants if expressed alone (data not shown). These results show that the binding site for ORF49p resides in the first third of ORF44p and that 129F plays a critical role in binding, either directly or indirectly. Furthermore, in GST-pulldown assays using GST-ORF44 (corresponding to aa 2 to 363), GST-ORF44F129A (aa 2 to 363 with F129A mutation), and GST-ORF44P (aa 180 to 363), only GST-ORF44 pulled down ORF49p expressed in and purified from MeWo cells (Fig. 4B), suggesting that there may not be a binding site within the C-terminal half of ORF44p; however, other C-terminal constructs have not been tested in this or other assays.

To analyze the impact of the 129F mutation in the context of infection, pOka-BACORF44T128A, pOka-BACORF44F129A, pOka-BACORF44K130A, and the revertant BAC for pOka-BACORF44F129A, pOka-BACORF44F129ARev, were generated (Fig. 1B). With the exception of the ORF44F129A mutant, the reconstitution of each virus with a mutation around 129F and of the revertant virus for the F129A mutant was successful, and all of the reconstituted viruses showed similar growth to rpOka (data not shown), suggesting that 129F of ORF44p may play a central role in the function of ORF44p in VZV infection, which occurs through its interaction with ORF49p.

The carboxyl-terminal half of the acidic cluster of ORF49p is required for the conserved interaction with ORF44p. To map the binding domain of ORF49p for ORF44p using the accumulation of ORF44p as an indicator of the interaction, we generated a series of carboxyl-terminal-truncated mutants of ORF49p (Fig. 1C). The coexpression of ORF44p and ORF49N48p or ORF49N44p resulted in the accumulation of ORF44p at the juxtanuclear region with TGN46 and the mutant ORF49p (Fig. 9A and B). In contrast, ORF44p never colocalized with ORF49N40p (Fig. 9C) and was dispersed in the cytoplasm, as when it was expressed alone (Fig. 5A). These results suggested that the ORF44p-binding domain in ORF49p may be located between the aspartate at aa 41 and glutamate at aa 44, which is in the carboxyl-terminal half of the conserved acidic cluster (Fig. 1C) in the ORF49 homologs.

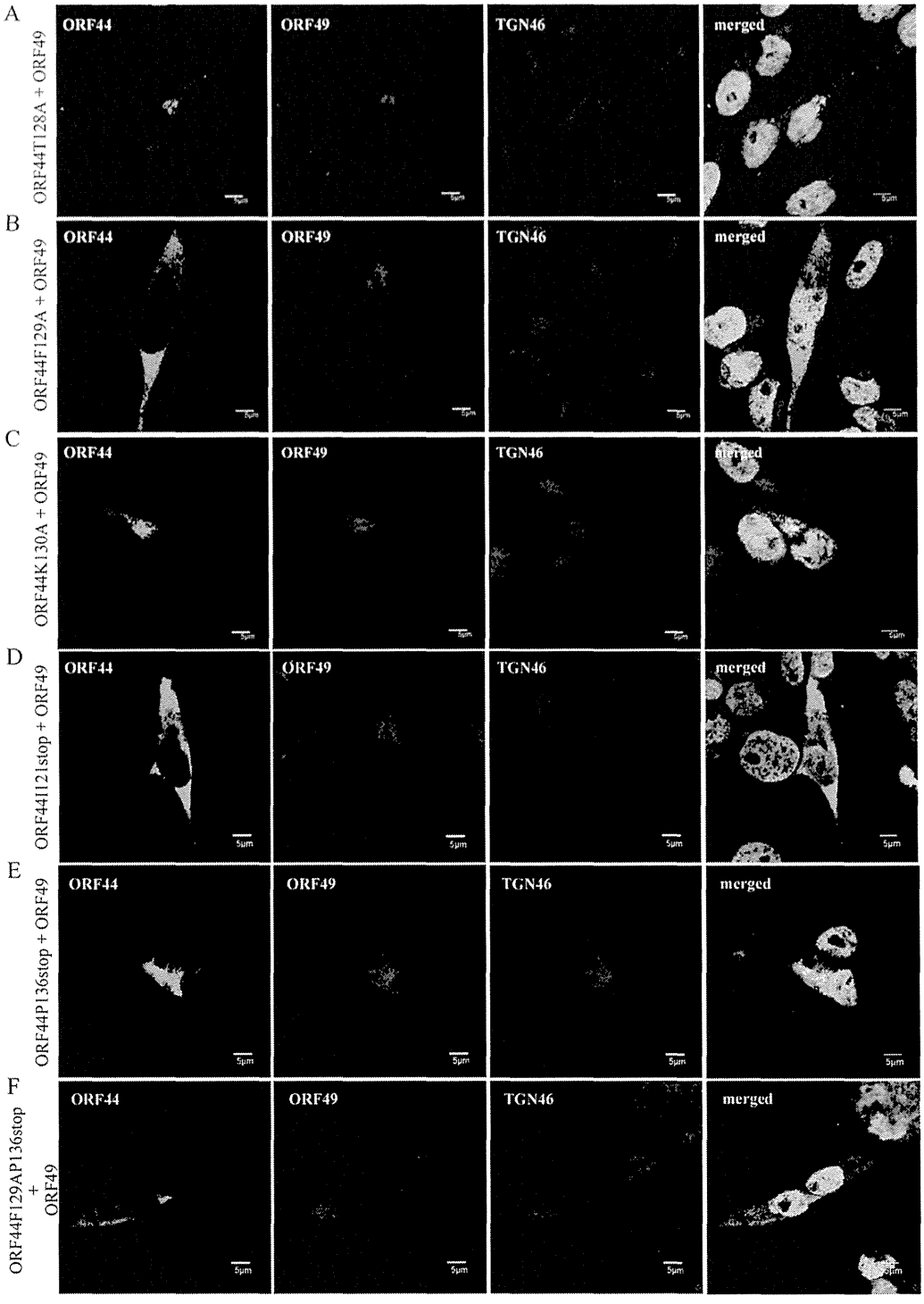

FIG 8 Localization and accumulation of ORF44 mutant proteins in MeWo cells expressing ORF49p. MeWo cells were cotransfected with CAG/ORF49 and CAG/ORF44T128A (A), CAG/ORF44F129A (B), CAG/ORF44K130A (C), CAG/FLAGORF44I121stop (D), CAG/FLAGORF44P136stop (E), or CAG/FLAGORF44F129AP136stop (F). Cells were fixed at 48 h posttransfection and triple labeled for ORF44 (green), ORF49 (red), and TGN46 (blue). Nuclei were stained with Hoechst 33342 (cyan). Scale bars, 5 μm.

To confirm the specificity of the ORF44p and ORF49p interaction while avoiding (although not excluding) nonspecific effects on the function of ORF49p resulting from the destruction of the ORF49p backbone, the four residues (41DFDE44) identified as the candidate ORF44p-binding motif were replaced by alanine, resulting in ORF49-41AAAA44p (Fig. 1C). As shown in Fig. 9D, ORF49-41AAAA44p targeted the TGN, similar to ORF49p (Fig. 5B), but it was unable to accumulate ORF44p on the TGN (Fig. 9E).

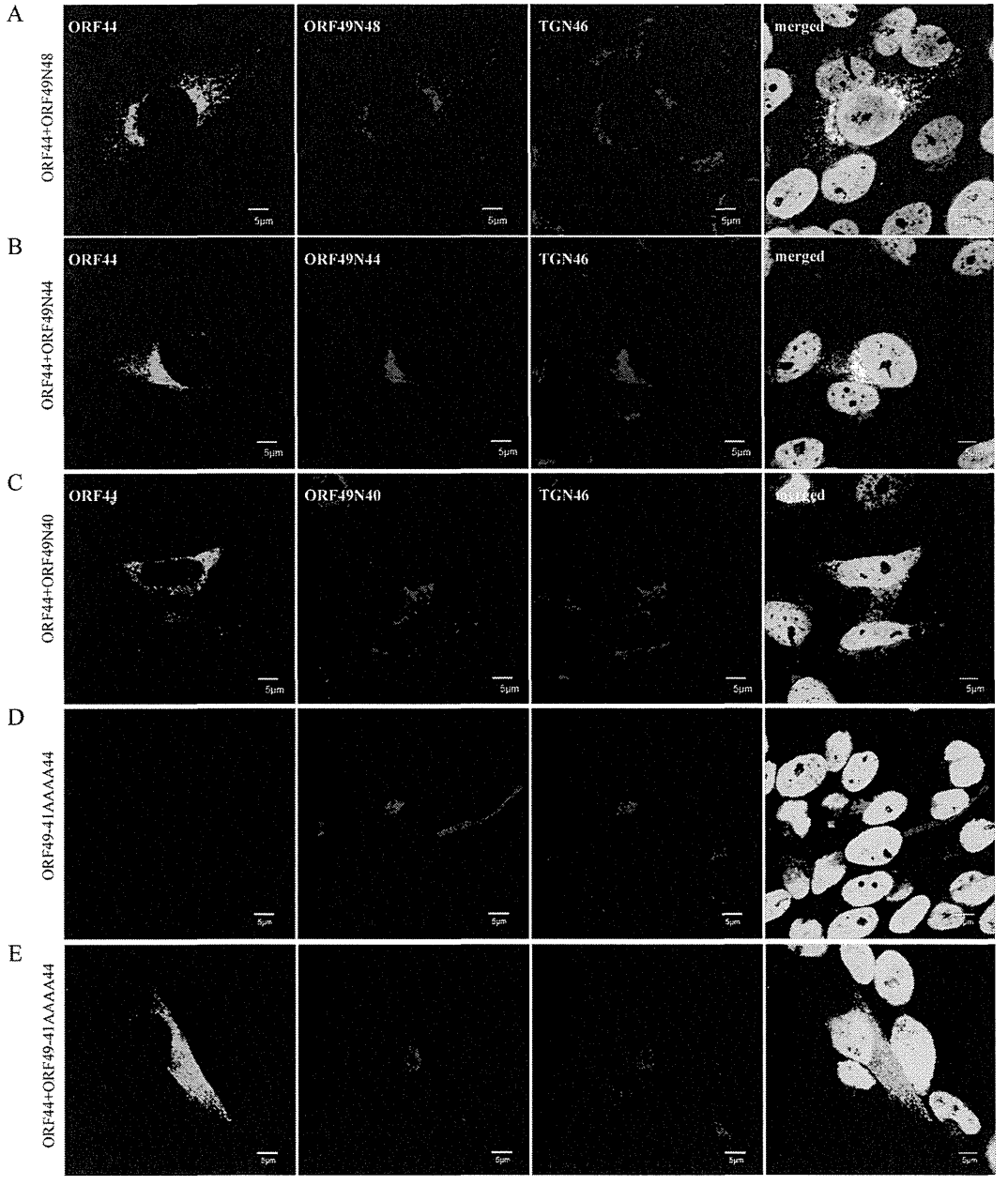

FIG 9 Localization and accumulation of ORF44p in MeWo cells expressing ORF49 mutant proteins. MeWo cells were cotransfected with CAG/ORF44 and CAG/ORF49N48 (A), CAG/ORF49N44 (B), CAG/ORF49N40 (C), or CAG/ORF49-41AAAA44 (E), or transfected with CAG/ORF49-41AAAA44 alone (D). Cells were fixed at 48 h posttransfection and triple labeled for ORF44 (green), ORF49 (red), and TGN46 (blue). Nuclei were stained with Hoechst 33342 (cyan). Scale bars, 5 μm.

Furthermore, ORF49-41AAAA44p did not form a complex with ORF44p or ORF44F129Ap (Fig. 6B, lane 5 or 6) despite the efficient coexpression of all proteins (Fig. 6A, lanes 5 and 6).

The carboxyl-terminal half of the acidic cluster of ORF49p plays a central role in the function of ORF49p during infection. rpOkaORF49-41AAAA44 showed almost the same phenotype as rpOkaORF49M1L, including the loss of the interaction with ORF44p (Fig. 2E, lane 1), the dispersed localization of ORF44p without accumulation on the TGN (Fig. 10A), impaired growth as assessed by plaque size and infectious-center assays (Fig. 11A and B, respectively), and reduced production of infectious progeny virus (to 3 to 10% of the wild-type level [Table 2]), excluding the apparent ORF49-41AAAA44p expression (Fig. 2D, lane 1, and Fig. 10A). These defects were completely rescued by revertant virus infection (Fig. 2D and E, lanes 2, Fig. 10B, and Fig. 11A and B) or by exogenous ORF49p in MeWoORF49 cells (Fig. 11A and B and Table 2). The expression of ORF49-41AAAA44p was detected as a faint and faster-migrating band than that of ORF49p in the revertant virus infection, but an equal amount of ORF44p was detected in both viruses with gH and ORF61p (Fig. 2D, lanes 1 and 2). Furthermore, whereas the interaction between ORF49-41AAAA44p and ORF44p was not detected at all (Fig. 2E, lane 1),

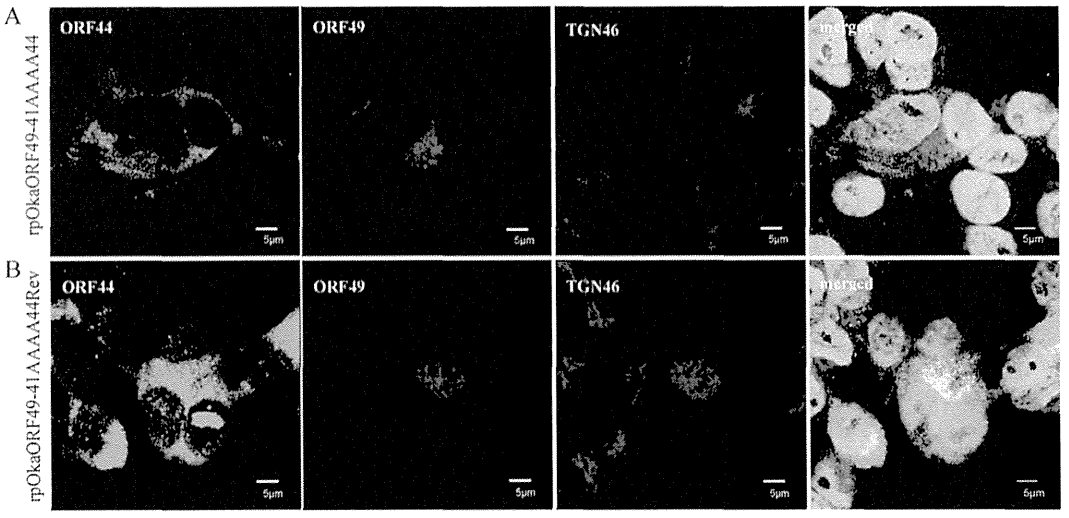

FIG 10 Localization of ORF44p and ORF49p in rpOkaORF49-41AAAA44-infected MeWo cells. rpOkaORF49-41AAAA44-infected MeWo cells (A) and rpOkaORF49-41AAAA44Rev-infected MeWo cells (B) were fixed at 48 hpi and triple labeled for ORF44p (green), ORF49p (red), and TGN46 (blue). Nuclei were stained with Hoechst 33342 (cyan). Scale bars, 5 μm.

ORF44p was incorporated into the rpOkaORF49-41AAAA44 particles in the absence or presence of exogenous ORF49p (Fig. 2F, lane 1 or 2), which was also the case in rpOkaORF49M1L infection (Fig. 2D and F).

Taken together, our results indicated that ORF49p functions in the efficient production of progeny viruses required for VZV infection through its interaction with the essential protein ORF44p.

DISCUSSION

In VZV, ORF49 encodes a nonessential tegument protein that is one of the cell-tropic factors in cell culture (6). In human fetal lung fibroblast MRC-5 cells, the growth of ORF49-defective virus is identical to that of its parental virus, whereas in the human melanoma MeWo cell line, it shows reduced growth; however, the cell tropism of VZV for these two most permissive cell lines has not been studied. In the previous study, we showed that it is a cell-tropic factor, although the step(s) at which ORF49 functions, including the entry, host gene modulation, viral gene expression, viral particle assembly, or egress, remained unclear. Nevertheless, we showed that it may play an important role in the production of a complete virion (6).

VZV is highly cell associated *in vitro*, producing extremely small amounts of infectious virus even when isolated intracellularly (in a particle-to-PFU ratio that varies from approximately 40,000 to 1,000,000) (39, 40), and the particles detected by electron microscopy (EM) analysis appear to be degraded, even in cells infected by the wild-type virus (41–43). The low infectivity and the presence of few or no infectious particles in the cell culture

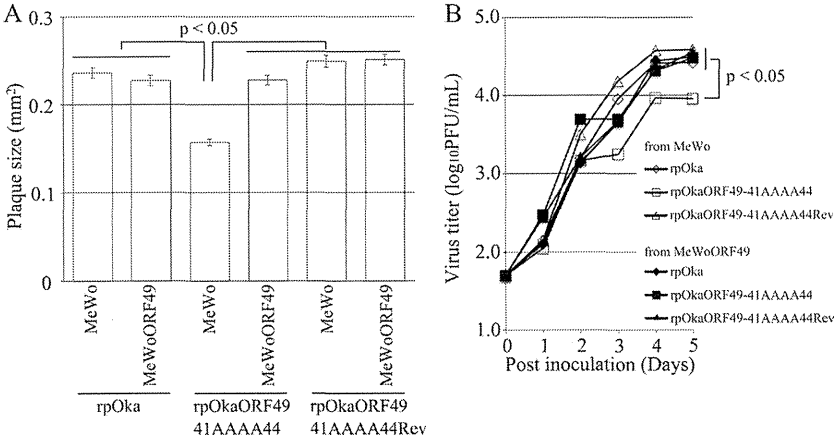

FIG 11 Growth properties of ORF49-41AAAA44 mutant virus in MeWo and MeWoORF49 cells. (A) Comparison of plaque sizes among recombinant viruses. MeWo cells or MeWoORF49 cells were infected with rpOka, rpOkaORF49-41AAAA44, or rpOkaORF49-41AAAA44Rev (50 PFU/well) and cultured for 7 days. Infected cells were stained with an anti-gE Ab, and the plaques were traced and measured by ImageJ software. Plaque size is shown with the standard error of the mean. Statistical significance was determined by Student's *t* test. (B) Growth kinetics of recombinant viruses on MeWo cells and MeWoORF49 cells. MeWo cells or MeWoORF49 cells were infected with rpOka, rpOkaORF49-41AAAA44, or rpOkaORF49-41AAAA44Rev (50 PFU/well), harvested at the indicated times, serially diluted, added to newly prepared MeWo cells, and cultured for 5 days. The plaques were stained with an anti-gE Ab and counted. Each point represents the mean titer for two wells of one experiment. Two experiments were performed independently. Statistical significance was determined by Student's *t* test.

supernatant in VZV have made it difficult to construct a *trans*-complementation system. In such a system, the target viral gene is expressed on permissive cells on which the target gene-deleted virus is only capable of efficient replication similar to the wild-type virus infection on the parental cells. The infection of parental cells by the target gene-deleted virus isolated from cells expressing the target gene enables analysis of its function. This method is useful to confirm that the deletion phenotype is not caused by undesired mutations, which can also be determined by generating the revertant virus to repair the mutated gene within the viral genome. In addition, it can also be used to identify the target gene function, which cannot be determined by simply generating the mutant and revertant viruses and has been used widely in the mutagenic analysis of other herpesviruses, especially in the analysis of structural proteins. However, to the best of our knowledge, this system has been used successfully to analyze gene function in only one report (44) and to confirm that the deletion phenotype is independent of undesired mutation in two reports (45, 46) in VZV research.

In the present study, we established a *trans*-complementation system for ORF49. The ORF49 *trans*-complementation system allowed identification of the precise function of ORF49, which could not be determined by generating its defective virus following EM analysis on MeWo cells. In the EM analysis, no significant differences between the wild-type and ORF49-defective viruses were detected with regard to the intracellular and cell surface viral particle counts or morphology (T. Sadaoka and Y. Mori, unpublished observation), possibly leading to their obvious difference in infectivity, which was reduced by 10-fold or higher in the defective virus. Additionally, in both viruses, the infected cells or viral particles isolated from the same quantity of infected cells contained almost the same amount of viral proteins. The *trans*-complementation system in combination with the results of other analyses described above indicated that ORF49 functions in the production of efficient infectious viruses. The results of EM analysis and immunoblotting suggested that the ORF49 defect did not cause the reduction of viral protein synthesis and viral particle assembly and egress. The cell-free virus titration and plaque formation analyses using the *trans*-complementation system showed that the ORF49p released from the virion into the cells during the entry step was not functional, but *de novo* ORF49p synthesized during lytic replication functioned in the production of efficient infectious virus required for cell-free and cell-to-cell viral transmission modes. However, how the deletion of ORF49 impaired infectivity remained unclear.

To gain further insight into the function of ORF49 during VZV infection, we confirmed ORF44p as its binding partner, as reported in other herpesviruses (12–15), and examined the conserved interaction between these proteins by analyzing their binding properties. We identified 129F in ORF44p as being essential for accumulation on the TGN through the interaction with ORF49p: whether it functions in the binding directly or indirectly is unknown. Simultaneously, 41DFDE44 of the carboxyl-terminal half of the acidic cluster within ORF49p was identified as the binding motif for ORF44p. Among these critical amino acids of ORF44p and ORF49p, each phenylalanine seems to function in the binding. As the phenylalanine is an aromatic and hydrophobic amino acid, it prefers to be buried in protein hydrophobic cores. However, 129F of ORF44p is surrounded by polar amino acid 128T and charged amino acid 130K and 42F of ORF49p by charged amino acids 41D, 43D, and 44E, and there is possibility that these two phenylalanines are exposed at the protein surface. The phenylalanine side chain is fairly nonreactive and is thus rarely directly involved in protein function, although it can play a role in substrate recognition. In particular, hydrophobic amino acids can be involved in binding/recognition of hydrophobic ligands, and the aromatic side chain can also be involved in interactions with other aromatic side chains via stacking interactions (47). In coexpression of ORF44 and ORF49, ORF49F42A mutation alone disrupted the interaction and failed to accumulate ORF44p on the TGN, as seen in ORF49-41AAAA44 mutation, while individual ORF49D41A, -D43A, or -E44A mutation had no effect on them (T. Sadaoka and Y. Mori, unpublished observation). On the other hand, ORF44F129A showed an impaired phenotype in terms of their interaction and its accumulation on the TGN, and neither ORF44T128A nor K130A mutation had any effect on them. However, in the context of infection, ORF49F42A alone could not abrogate the interaction and had no effect on virus growth (T. Sadaoka and Y. Mori, unpublished observation) different from that of ORF49-41AAAA44 mutation (discussed below), while only ORF44F129A was truly lethal for infectious virus production/reconstitution, and again ORF44T128A and ORF44K130A had no effect. These findings may prompt us to conclude that the core machinery of the binding is the noncovalent attractive force between two aromatic rings of phenylalanine and that the additional binding force via charged amino acids around 42F of ORF49p is required in the context of infection; however, there is another possibility—that the ORF44F129A mutation just disrupts the protein structure itself, leading to the loss of interaction. As mentioned above, phenylalanine prefers to be buried in protein hydrophobic cores, and the interaction among the aromatic residues is also important in the protein folding and the structural stabilization of protein (48, 49). Our results about the interaction property revealed that the binding domain within ORF44p is located at the first 136 residues and 129F is essentially involved in the binding, but could not be determined as the precise binding domain, and at the same time, there was no apparent degradation or lower expression of ORF44F129Ap in comparison with ORF44p in both prokaryotic expression and eukaryotic expression systems. To address these issues, further analyses by making an N-terminal truncation for refining the interaction domain and another 129F substitution with tyrosine, which differs only in that it contains a hydroxyl group in place of the ortho hydrogen on the benzene ring, for more preferable substitution to maintain structural stability will be helpful and ongoing.

Assessment of the function of ORF44 in the context of infection did not reveal new findings, with the exception of the F129A mutant, which showed the same phenotype as the deletion mutant. The ORF44 deletion and F129A mutation were lethal for progeny virus production/reconstitution in MeWo and MRC-5 cells; however, an effective *trans*-complementation system for ORF44 as for ORF49 was not successfully established, and at what step(s) in the lytic infection ORF44 essentially functions remained unclear. To find the nonessential but important functions of ORF44 in the context of infection, we turned back to analyzing the ORF49 function by generating ORF49-41AAAA44 virus, in which ORF49p specifically lost the interaction with ORF44p, following comparison of the phenotype between ORF49-defective virus and ORF49-41AAAA44 virus. The rpOkaORF49-41AAAA44 virus showed the same phenotype as the rpOkaORF49M1L virus, indicating that the function of ORF49p in the efficient production of

progeny viruses was completely dependent on the interaction with ORF44p at 41DFDE44. These results suggest that ORF44p is fully functional only in the presence of ORF49p and vice versa and has essential functions during infection, which are independent of the interaction with ORF49p or redundantly supported by other viral factors in the absence of ORF49p.

In the absence of the interaction with ORF49p during infection, ORF44p was detected throughout the cytoplasm and rarely colocalized with the TGN (or with a reorganized organ containing TGN-derived membranes known to be induced by viral infection, although it has not been found in VZV infection), the recognized site of viral assembly; however, incorporation of ORF44p into viral particles was comparable to that observed in wild-type virus infection. These results indicate that ORF44p was not directly incorporated into the particles through the TGN via its interaction with ORF49p, at least in the absence of ORF49p. In HSV-1, the amount of pUL16 packaged into the viral particles was severely reduced in the absence of pUL11 (50), but there are some other interaction partners that potentially function in incorporating pUL16 into the viral particles (i.e., pUL21 and glycoprotein E) (51, 52). In VZV, by global screening using the yeast two-hybrid system, some candidates for ORF44p binding partner have been reported (28, 29), but in our observations, none of these viral proteins other than ORF49p could accumulate ORF44p on the TGN; one viral protein could alter the localization of ORF44p into the nucleus; however, whether it functions in the incorporation of ORF44p into the viral particles remained unclear (T. Sadaoka and Y. Mori, unpublished observation). Anyway, additional ORF44p binding partners active during either the wild-type virus or ORF49-defective virus infection remain to be identified so far, and the complexity of the herpesvirus protein-protein network requires a solid approach to elucidate the essential roles of ORF44 during viral infection further through the interactions with other viral proteins.

In summary, in the present study, we established a *trans*-complementation system for ORF49 and identified ORF44p as the binding partner for ORF49p. We showed that (i) ORF49p functions in the efficient production of infectious virus, (ii) no other viral factor is required for binding, (iii) residue 129F of ORF44p is critical not only for binding to ORF49p but also for progeny virus production/reconstitution, (iv) the carboxyl-terminal half of the acidic cluster (41DFDE44) of ORF49p is the binding motif for ORF44p, and (v) the efficient production of infectious progeny virus by ORF49p is dependent on its interaction with ORF44p. Further analyses of the role of ORF44 mediated by its interaction with ORF49 or other as yet unidentified viral proteins may shed light on the conserved infection mechanisms of the *Herpesvirinae* and those unique to VZV.

ACKNOWLEDGMENTS

We thank Eiko Moriishi (National Institute of Biomedical Innovation, Osaka, Japan) for technical assistance, Panayiotis A. Ioannou (Cell and Gene Therapy Research Group, The Murdoch Children's Research Institute, The University of Melbourne, Royal Children's Hospital, Melbourne, Australia) for providing pGETrec, Wilfried Wackernagel (Genetics, Department of Biology and Environmental Sciences, Universität Oldenburg, Germany) for pCP20, Jun-ichi Miyazaki (Division of Stem Cell Regulation Research, Osaka University Graduate School of Medicine, Japan) for pCAGGS, Masaru Okabe (Department of Experimental Genome Research, Genome Information Research Center, Osaka University, Japan) for pCX-Cre, and Ulrich H. Koszinowski (Max von Pettenkofer Institut fur Virologie, Ludwig-Maximilians-Universität München, Germany) for pHA2 and pST76A-SR.

This study was supported in part by a Grant-in-Aid for Scientific Research on Priority Areas (21022031 to Y.M.) from the Ministry of Education, Culture, Sports, Science, and Technology (MEXT) of Japan, a Grant-in-Aid for Scientific Research (B) (20390138 to Y.M.), a Grant-in-Aid for Young Scientists (B) (20790363 and 22790432 to T.S.), a Grant-in-Aid for Scientific Research (C) (24590551 to T.S.) from the Japan Society for the Promotion of Science (JSPS), and a grant from the Uehara Memorial Foundation (to T.S.).

REFERENCES

1. **Moffat J, Ku CC, Zerboni L, Sommer M, Arvin A.** 2007. VZV: pathogenesis and the disease consequences of primary infection, p 675–688. *In* Arvin A, Campadelli-Fiume G, Mocarski E, Moore PS, Roizman B, Whitley R, Yamanishi K (ed), Human herpesviruses: biology, therapy, and immunoprophylaxis. Cambridge University Press, Cambridge, United Kingdom.
2. **Baines JD, Pellett PE.** 2007. Genetic comparison of human alphaherpesvirus genomes, p 61–69. *In* Arvin A, Campadelli-Fiume G, Mocarski E, Moore PS, Roizman B, Whitley R, Yamanishi K (ed), Human herpesviruses: biology, therapy, and immunoprophylaxis. Cambridge University Press, Cambridge, United Kingdom.
3. **Davison AJ, Scott JE.** 1986. The complete DNA sequence of varicella-zoster virus. J. Gen. Virol. **67**:1759–1816. http://dx.doi.org/10.1099/0022-1317-67-9-1759.
4. **Davison AJ.** 2007. Comparative analysis of the genomes, p 10–26. *In* Arvin A, Campadelli-Fiume G, Mocarski E, Moore PS, Roizman B, Whitley R, Yamanishi K (ed), Human herpesviruses: biology, therapy, and immunoprophylaxis. Cambridge University Press, Cambridge, United Kingdom.
5. **Zhang Z, Selariu A, Warden C, Huang G, Huang Y, Zaccheus O, Cheng T, Xia N, Zhu H.** 2010. Genome-wide mutagenesis reveals that ORF7 is a novel VZV skin-tropic factor. PLoS Pathog. **6**:e1000971. http://dx.doi.org/10.1371/journal.ppat.1000971.
6. **Sadaoka T, Yoshii H, Imazawa T, Yamanishi K, Mori Y.** 2007. Deletion in open reading frame 49 of varicella-zoster virus reduces virus growth in human malignant melanoma cells but not in human embryonic fibroblasts. J. Virol. **81**:12654–12665. http://dx.doi.org/10.1128/JVI.01183-07.
7. **Baines JD, Jacob RJ, Simmerman L, Roizman B.** 1995. The herpes simplex virus 1 UL11 proteins are associated with cytoplasmic and nuclear membranes and with nuclear bodies of infected cells. J. Virol. **69**:825–833.
8. **Britt WJ, Jarvis M, Seo JY, Drummond D, Nelson J.** 2004. Rapid genetic engineering of human cytomegalovirus by using a lambda phage linear recombination system: demonstration that pp28 (UL99) is essential for production of infectious virus. J. Virol. **78**:539–543. http://dx.doi.org/10.1128/JVI.78.1.539-543.2004.
9. **Silva MC, Yu QC, Enquist L, Shenk T.** 2003. Human cytomegalovirus UL99-encoded pp28 is required for the cytoplasmic envelopment of tegument-associated capsids. J. Virol. **77**:10594–10605. http://dx.doi.org/10.1128/JVI.77.19.10594-10605.2003.
10. **MacLean CA, Dolan A, Jamieson FE, McGeoch DJ.** 1992. The myristylated virion proteins of herpes simplex virus type 1: investigation of their role in the virus life cycle. J. Gen. Virol. **73**:539–547. http://dx.doi.org/10.1099/0022-1317-73-3-539.
11. **Silva MC, Schroer J, Shenk T.** 2005. Human cytomegalovirus cell-to-cell spread in the absence of an essential assembly protein. Proc. Natl. Acad. Sci. U. S. A. **102**:2081–2086. http://dx.doi.org/10.1073/pnas.0409597102.
12. **Loomis JS, Courtney RJ, Wills JW.** 2003. Binding partners for the UL11 tegument protein of herpes simplex virus type 1. J. Virol. **77**:11417–11424. http://dx.doi.org/10.1128/JVI.77.21.11417-11424.2003.
13. **Guo H, Wang L, Peng L, Zhou ZH, Deng H.** 2009. Open reading frame 33 of a gammaherpesvirus encodes a tegument protein essential for virion morphogenesis and egress. J. Virol. **83**:10582–10595. http://dx.doi.org/10.1128/JVI.00497-09.
14. **Liu Y, Cui Z, Zhang Z, Wei H, Zhou Y, Wang M, Zhang XE.** 2009. The tegument protein UL94 of human cytomegalovirus as a binding partner for tegument protein pp28 identified by intracellular imaging. Virology **388**:68–77. http://dx.doi.org/10.1016/j.virol.2009.03.007.
15. **Maninger S, Bosse JB, Lemnitzer F, Pogoda M, Mohr CA, von Einem J, Walther P, Koszinowski UH, Ruzsics Z.** 2011. M94 is essential for the

secondary envelopment of murine cytomegalovirus. J. Virol. 85:9254–9267. http://dx.doi.org/10.1128/JVI.00443-11.
16. Meckes DG, Jr, Wills JW. 2007. Dynamic interactions of the UL16 tegument protein with the capsid of herpes simplex virus. J. Virol. 81:13028–13036. http://dx.doi.org/10.1128/JVI.01306-07.
17. Nalwanga D, Rempel S, Roizman B, Baines JD. 1996. The UL 16 gene product of herpes simplex virus 1 is a virion protein that colocalizes with intranuclear capsid proteins. Virology 226:236–242. http://dx.doi.org/10.1006/viro.1996.0651.
18. Oshima S, Daikoku T, Shibata S, Yamada H, Goshima F, Nishiyama Y. 1998. Characterization of the UL16 gene product of herpes simplex virus type 2. Arch. Virol. 143:863–880. http://dx.doi.org/10.1007/s007050050338.
19. Yeh PC, Meckes DG, Jr, Wills JW. 2008. Analysis of the interaction between the UL11 and UL16 tegument proteins of herpes simplex virus. J. Virol. 82:10693–10700. http://dx.doi.org/10.1128/JVI.01230-08.
20. Johnson DC, Baines JD. 2011. Herpesviruses remodel host membranes for virus egress. Nat. Rev. Microbiol. 9:382–394. http://dx.doi.org/10.1038/nrmicro2559.
21. Baines JD, Roizman B. 1991. The open reading frames UL3, UL4, UL10, and UL16 are dispensable for the replication of herpes simplex virus 1 in cell culture. J. Virol. 65:938–944.
22. Dunn W, Chou C, Li H, Hai R, Patterson D, Stolc V, Zhu H, Liu F. 2003. Functional profiling of a human cytomegalovirus genome. Proc. Natl. Acad. Sci. U. S. A. 100:14223–14228. http://dx.doi.org/10.1073/pnas.2334032100.
23. Klupp BG, Bottcher S, Granzow H, Kopp M, Mettenleiter TC. 2005. Complex formation between the UL16 and UL21 tegument proteins of pseudorabies virus. J. Virol. 79:1510–1522. http://dx.doi.org/10.1128/JVI.79.3.1510-1522.2005.
24. Phillips SL, Bresnahan WA. 2012. The human cytomegalovirus (HCMV) tegument protein UL94 is essential for secondary envelopment of HCMV virions. J. Virol. 86:2523–2532. http://dx.doi.org/10.1128/JVI.06548-11.
25. Yu D, Silva MC, Shenk T. 2003. Functional map of human cytomegalovirus AD169 defined by global mutational analysis. Proc. Natl. Acad. Sci. U. S. A. 100:12396–12401. http://dx.doi.org/10.1073/pnas.1635160100.
26. Chadha P, Han J, Starkey JL, Wills JW. 2012. Regulated interaction of tegument proteins UL16 and UL11 from herpes simplex virus. J. Virol. 86:11886–11898. http://dx.doi.org/10.1128/JVI.01879-12.
27. Phillips SL, Cygnar D, Thomas A, Bresnahan WA. 2012. Interaction between the human cytomegalovirus tegument proteins UL94 and UL99 is essential for virus replication. J. Virol. 86:9995–10005. http://dx.doi.org/10.1128/JVI.01078-12.
28. Stellberger T, Hauser R, Baiker A, Pothineni VR, Haas J, Uetz P. 2010. Improving the yeast two-hybrid system with permutated fusions proteins: the varicella zoster virus interactome. Proteome Sci. 8:8. http://dx.doi.org/10.1186/1477-5956-8-8.
29. Uetz P, Dong YA, Zeretzke C, Atzler C, Baiker A, Berger B, Rajagopala SV, Roupelieva M, Rose D, Fossum E, Haas J. 2006. Herpesviral protein networks and their interaction with the human proteome. Science 311:239–242. http://dx.doi.org/10.1126/science.1116804.
30. Sadaoka T, Yanagi T, Yamanishi K, Mori Y. 2010. Characterization of the varicella-zoster virus ORF50 gene, which encodes glycoprotein M. J. Virol. 84:3488–3502. http://dx.doi.org/10.1128/JVI.01838-09.
31. Niwa H, Yamamura K, Miyazaki J. 1991. Efficient selection for high-expression transfectants with a novel eukaryotic vector. Gene 108:193–199. http://dx.doi.org/10.1016/0378-1119(91)90434-D.
32. Sadaoka T, Yamanishi K, Mori Y. 2006. Human herpesvirus 7 U47 gene products are glycoproteins expressed in virions and associate with glycoprotein H. J. Gen. Virol. 87:501–508. http://dx.doi.org/10.1099/vir.0.81374-0.
33. Okuno T, Yamanishi K, Shiraki K, Takahashi M. 1983. Synthesis and processing of glycoproteins of varicella-zoster virus (VZV) as studied with monoclonal antibodies to VZV antigens. Virology 129:357–368. http://dx.doi.org/10.1016/0042-6822(83)90175-7.
34. Nagaike K, Mori Y, Gomi Y, Yoshii H, Takahashi M, Wagner M, Koszinowski U, Yamanishi K. 2004. Cloning of the varicella-zoster virus genome as an infectious bacterial artificial chromosome in Escherichia coli. Vaccine 22:4069–4074. http://dx.doi.org/10.1016/j.vaccine.2004.03.062.
35. Narayanan K, Williamson R, Zhang Y, Stewart AF, Ioannou PA. 1999. Efficient and precise engineering of a 200 kb beta-globin human/bacterial artificial chromosome in E. coli DH10B using an inducible homologous recombination system. Gene Ther. 6:442–447. http://dx.doi.org/10.1038/sj.gt.3300901.
36. Cherepanov PP, Wackernagel W. 1995. Gene disruption in Escherichia coli: TcR and KmR cassettes with the option of Flp-catalyzed excision of the antibiotic-resistance determinant. Gene 158:9–14. http://dx.doi.org/10.1016/0378-1119(95)00193-A.
37. Hobom U, Brune W, Messerle M, Hahn G, Koszinowski UH. 2000. Fast screening procedures for random transposon libraries of cloned herpesvirus genomes: mutational analysis of human cytomegalovirus envelope glycoprotein genes. J. Virol. 74:7720–7729. http://dx.doi.org/10.1128/JVI.74.17.7720-7729.2000.
38. Shevchenko A, Wilm M, Vorm O, Mann M. 1996. Mass spectrometric sequencing of proteins silver-stained polyacrylamide gels. Anal. Chem. 68:850–858. http://dx.doi.org/10.1021/ac950914h.
39. Carpenter JE, Henderson EP, Grose C. 2009. Enumeration of an extremely high particle-to-PFU ratio for varicella-zoster virus. J. Virol. 83:6917–6921. http://dx.doi.org/10.1128/JVI.00081-09.
40. Shiraki K, Takahashi M. 1982. Virus particles and glycoprotein excreted from cultured cells infected with varicella-zoster virus (VZV). J. Gen. Virol. 61:271–275. http://dx.doi.org/10.1099/0022-1317-61-2-271.
41. Gabel CA, Dubey L, Steinberg SP, Sherman D, Gershon MD, Gershon AA. 1989. Varicella-zoster virus glycoprotein oligosaccharides are phosphorylated during posttranslational maturation. J. Virol. 63:4264–4276.
42. Gershon AA, Sherman DL, Zhu Z, Gabel CA, Ambron RT, Gershon MD. 1994. Intracellular transport of newly synthesized varicella-zoster virus: final envelopment in the trans-Golgi network. J. Virol. 68:6372–6390.
43. Harson R, Grose C. 1995. Egress of varicella-zoster virus from the melanoma cell: a tropism for the melanocyte. J. Virol. 69:4994–5010.
44. Ali MA, Li Q, Fischer ER, Cohen JI. 2009. The insulin degrading enzyme binding domain of varicella-zoster virus (VZV) glycoprotein E is important for cell-to-cell spread and VZV infectivity, while a glycoprotein I binding domain is essential for infection. Virology 386:270–279. http://dx.doi.org/10.1016/j.virol.2009.01.023.
45. Tischer BK, Kaufer BB, Sommer M, Wussow F, Arvin AM, Osterrieder N. 2007. A self-excisable infectious bacterial artificial chromosome clone of varicella-zoster virus allows analysis of the essential tegument protein encoded by ORF9. J. Virol. 81:13200–13208. http://dx.doi.org/10.1128/JVI.01148-07.
46. Yamagishi Y, Sadaoka T, Yoshii H, Somboonthum P, Imazawa T, Nagaike K, Ozono K, Yamanishi K, Mori Y. 2008. Varicella-zoster virus glycoprotein M homolog is glycosylated, is expressed on the viral envelope, and functions in virus cell-to-cell spread. J. Virol. 82:795–804. http://dx.doi.org/10.1128/JVI.01722-07.
47. Betts MJ, Russell RB. 22 May 2003. Amino acid properties and consequences of substitutions. Chapter 14. *In* Barnes MR, Gray IC (ed), Bioinformatics for geneticists. Wiley, Chichester, West Sussex, England. http://dx.doi.org/10.1002/0470867302.ch14.
48. Burley SK, Petsko GA. 1985. Aromatic-aromatic interaction: a mechanism of protein structure stabilization. Science 229:23–28. http://dx.doi.org/10.1126/science.3892686.
49. Eidenschink LA, Kier BL, Andersen NH. 2009. Determinants of fold stabilizing aromatic-aromatic interactions in short peptides. Adv. Exp. Med. Biol. 611:73–74. http://dx.doi.org/10.1007/978-0-387-73657-0_32.
50. Meckes DG, Jr, Marsh JA, Wills JW. 2010. Complex mechanisms for the packaging of the UL16 tegument protein into herpes simplex virus. Virology 398:208–213. http://dx.doi.org/10.1016/j.virol.2009.12.004.
51. Han J, Chadha P, Meckes DG, Jr, Baird NL, Wills JW. 2011. Interaction and interdependent packaging of tegument protein UL11 and glycoprotein E of herpes simplex virus. J. Virol. 85:9437–9446. http://dx.doi.org/10.1128/JVI.05207-11.
52. Harper AL, Meckes DG, Jr, Marsh JA, Ward MD, Yeh PC, Baird NL, Wilson CB, Semmes OJ, Wills JW. 2010. Interaction domains of the UL16 and UL21 tegument proteins of herpes simplex virus. J. Virol. 84:2963–2971. http://dx.doi.org/10.1128/JVI.02015-09.

Microbiology and Immunology

Microbiol Immunol 2014; 58: 119–125
doi: 10.1111/1348-0421.12121

ORIGINAL ARTICLE

MHC class I molecules are incorporated into human herpesvirus-6 viral particles and released into the extracellular environment

Megumi Ota[1], Satoshi Serada[2], Tetsuji Naka[2] and Yasuko Mori[1]

[1]Division of Clinical Virology, Center for Infectious Diseases, Kobe University Graduate School of Medicine, 7-5-1, Kusunoki-cho, Chuo-ku, Kobe 650-0017, Japan and [2]Laboratory of Immune Signal, Division of Biomedical Research, National Institute of Biomedical Innovation, 7-6-8, Saito-Asagi, Ibaraki, Osaka 567-0085, Japan

ABSTRACT

Human herpesvirus-6 (HHV-6), which belongs to the betaherpesvirus subfamily, mainly replicates in T lymphocytes. Here, we show that MHC class I molecules are incorporated into HHV-6 viral particles and released into the extracellular environment. In addition, HHV-6A/B-infected T cells showed reduced surface and intracellular expression of MHC class I molecules. The cellular machinery responsible for molecular transport appears to be modified upon HHV-6 infection, causing MHC class I molecules to be transported to virion assembly sites.

Key words human herpesvirus-6A/B, MHC class I, viral particles.

Human herpesvirus 6 (HHV-6), which belongs to the betaherpesvirus subfamily (1), was first isolated from peripheral blood lymphocytes obtained from patients with lymphoproliferative disorders (2). HHV-6 isolates are classified as HHV-6A and HHV-6B based on genetic and antigenic differences and their cell tropism (2–5). Primary infection with HHV-6B causes exanthem subitum (6). The diseases caused by HHV-6A are so far unknown. HHV-6B mostly infects infants and remains latent in more than 90% of the population (7).

In general, herpesviruses use several strategies to evade host immune responses. For example, viruses may inhibit MHC class I-associated antigen presentation to escape detection by cytotoxic T lymphocytes. Several proteins expressed by herpesviruses block the transport of antigenic peptides from the cytosol to the endoplasmic reticulum (8–11), whereas others retain (12–14) or destroy class I molecules, or deliver them to lysosomes for degradation (15–18). The result is reduced surface expression of MHC class I molecules, enabling the virus to evade host immune surveillance.

HHV-6A, but not HHV-6B, downregulates expression of MHC class I in dendritic cells (19). HHV-6 U21 binds to and diverts MHC class I molecules to an endolysosomal compartment, effectively removing them from the cell surface and providing a possible means of immune escape (20).

Here, we show that expression of MHC class I molecules by infected cells is downregulated with incorporation into HHV-6 viral particles, suggesting a possible mechanism by which the virus escapes host immune surveillance.

MATERIALS AND METHODS

Cells and viruses

CBMCs were prepared as described previously (21). CBMCs were provided by K. Adachi (Minoh Hospital, Minoh,

Correspondence
Yasuko Mori, Division of Clinical Virology, Center for Infectious Diseases, Kobe University Graduate School of Medicine, 7-5-1, Kusunoki-cho, Chuo-ku, Kobe 650-0017, Japan.
Tel: +81 78 382 6878; fax: +81 78 382 6879; email: ymori@med.kobe-u.ac.jp

Received 17 October 2013; revised 22 November 2013; accepted 6 December 2013.

List of Abbreviations: CBMC, umbilical cord blood mononuclear cell; LC-MS/MS, liquid chromatography-tandem mass spectrometry; HHV-6A, human herpesvirus-6A; HHV-6B, human herpesvirus-6B; MVB, multivesicular body; TGN, *trans*-Golgi network.

Japan) and H. Yamada (Kobe University Graduate School of Medicine, Kobe, Japan) and purchased from the Cell Bank of the RIKEN BioResource Center, Tsukuba, Japan. Virus stocks were also prepared as described previously (21, 22). HSB-2 and MT-4 cell lines were used in this study (23). HHV-6A (strain GS) and HHV-6B (strain HST) were prepared as previously described (21).

Antibodies

Monoclonal antibody (Mab) OHV-1 (24) and a polyclonal antibody against gB (23, 25) have been described previously. The following other Mabs were purchased: MHC class I (clone: W6/32; Bio Legend, San Diego, CA, USA), CD63 (clone: CLB-gran/12, 435; Sanquin Blood Supply, Amsterdam, the Netherlands), and α-tubulin (clone: B-5-1-2; Sigma, St Louis, MO, USA). The following secondary antibodies were used: Alexa Fluor 488- or 594-conjugated F(ab′)2 fragment of goat anti-mouse or rabbit immunoglobulin G (IgG) (Invitrogen, Tokyo, Japan) and anti-mouse IgG, horseradish peroxidase-linked whole antibody (from sheep) (GE Healthcare, Piscataway, NJ, USA).

Virion and exosome isolation

Virions and exosomes were purified as previously described (23, 26). The collected fractions were used for western blotting, electron microscopy or liquid chromatography-tandem mass spectrometry (LC-MS/MS).

Liquid chromatography-tandem mass spectrometry

The fractions described above were analyzed by LC-MS/MS. Proteins were diluted tenfold with 9.8 M urea. The solutions were adjusted to pH 8.5, reduced with 13 mM dithiothreitol at 37°C for 1.5 hr and alkylated with 27 mM iodoacetamide in the dark for 1 hr. The protein mixtures were further diluted with 100 mM triethylammonium bicarbonate (pH 8.5) to reduce urea to 1 M, and digested with 4 μL of 1 mg/mL trypsin–tosyl phenylalanyl chloromethyl ketone solution. Samples were digested overnight at 37°C. Following digestion, lysates were acidified by adding 10% trifluoroacetic acid. The samples were desalted using peptide cleanup C18 spin tubes (Agilent Technologies, Santa Clara, CA, USA) and vacuum-dried. NanoLC-MS/MS analyses were performed on an LTQ-Orbitrap XL mass spectrometer (Thermo Fisher Scientific, Waltham, MA, USA) as described previously (27), while spray voltage was changed to 1800 V. Peptides and proteins were identified by automated database searches using Proteome Discoverer v.1.1 (Thermo Fisher Scientific) against all entries of the Swiss Prot protein database (version 3.26) with a precursor mass tolerance of 10 p.p.m., a fragment ion mass tolerance of 0.8 Da, and strict trypsin specificity, allowing for up to two missed cleavages. Cysteine carbamidomethylation was set as a fixed modification, and methionine oxidation was allowed as a variable modification.

Western blotting

Western blotting was performed as described previously (28, 29).

Electron microscopy

Electron microscopy was performed as described previously (30).

Briefly, the virion-containing pellets were resuspended in 2% (w/v) paraformaldehyde solution buffered with 0.1 M phosphate (pH 7.2). Next, 5 μL of the resuspended pellet was loaded onto formvar–carbon-coated grids to adsorb the virions. Immunostaining was then performed. The virions were incubated with mouse anti-gB, anti-MHC class I or anti-CD63 antibody for 1 hr at room temperature, followed by goat anti-mouse IgG conjugated to 10 nm colloidal gold particles (GE Healthcare) for a further 1 hr at room temperature. After immunolabeling, the samples were washed in distilled water, stained for 5 min with uranyl oxalate, pH 7.0, washed again, embedded in a mixture of 1.8% methylcellulose and 0.4% uranyl acetate, pH 4.0, at 4°C, air-dried, and observed under a Hitachi H-7100 electron microscope (Hitachi, Tokyo, Japan). For the control experiments, samples were incubated with the secondary antibody alone.

Flow cytometry

MT-4 cells were infected with HHV-6B. At 72 hr post-infection, the cells were fixed with 4% (w/v) paraformaldehyde at room temperature for 15 min and incubated with anti-MHC class I Mab at 37°C for 1 hr. The cells were then stained with an appropriate secondary antibody at 37°C for 30 min. For the control experiments, samples were incubated with the secondary antibody alone. Stained cells were analyzed using a flow cytometer (ec800; Sony, Tokyo, Japan).

Immunofluorescence assay

Immunofluorescence assay was performed as described previously (28). Briefly, MT-4 cells were infected with HHV-6B. At 72 hr post-infection, the cells were fixed with cold acetone–methanol (7:3) and incubated at 37°C

for 1 hr with an anti-HHV-6 gB rabbit antibody or an anti-MHC class I Mab. After washing for 10 min with PBS containing 0.02% Tween-20, the cells were incubated with an appropriate secondary antibody at 37°C for 30 min, followed by Hoechst33342 at 37°C for 40 min. After washing as described above, signals were detected by a confocal laser-scanning microscope (Olympus FluoView FV1000; Olympus, Tokyo, Japan).

RESULTS

Virion and exosome isolation

Extracellular viral particles containing exosomes were purified from the culture supernatant of HHV-6A (strain GS)-infected HSB-2 or HHV-6B (strain HST)-infected MT-4 cells. The particle-containing fractions were confirmed by western blotting with an anti-gB antibody (23, 25). Next, the particle-containing fractions were analyzed by LC-MS/MS (27), which detected many cellular proteins (unpublished data). Of the host proteins detected, our analyses focused on MHC class I molecules.

Virion- or exosome-associated fractions contain MHC class I molecules

To verify expression of MHC class I within viral particles, the proteins in fractions 3–10 were separated by SDS–PAGE and analyzed by western blotting with anti-gB rabbit, anti-MHC class I or anti-CD63 antibodies. As shown in Figure 1, gB protein was detected in fractions 5–6 whereas MHC class I was detected primarily in fractions 6–8. We have previously reported that the MVB marker, CD63, is incorporated into virions and exosomes (23); therefore, expression of CD63 was also examined. As expected, CD63 was detected in fractions 5–10 (Fig. 1c). To confirm expression of MHC class I within both virions and exosomes, negative staining of fractions 6 and 7 were performed, followed by electron microscopy (30). Fraction 6 contained mainly viral particles of diameter approximately 200 nm. Both MHC class I (Fig. 1e) and gB protein (Fig. 1d) were present in these particles. Fraction 7 contained mainly exosomes of diameter approximately 50–100 nm (Fig. 1f). These exosomes contained MHC class I, which confirmed the results of the western blotting experiments. Taken together, these results indicate that MHC class I molecules are present in exosomes and virions released from HHV-6B-infected cells.

Downregulated expression of MHC class I molecules on the surface of HHV-6B-infected cells

Downregulation of MHC class I occurs in many different virus-infected cells (31–37). Because MHC class I molecules were incorporated into virions, HHV-6-infected MT-4 cells might show an apparent downregulation in cell surface expression. To confirm this, HHV-6B- or mock-infected cells harvested 72 hr post-infection were fixed and then stained with an anti-MHC class I antibody. Surface expression of MHC class I was then analyzed by flow cytometry. As expected, HHV-6B-infected cells showed downregulated cell surface expression of MHC class I when compared with mock-infected cells (Fig. 2a). This reduced expression was confirmed by western blot analysis (Fig. 2b), indicating that expression of MHC class I molecules within HHV-6-infected cells (not just expression on the cell surface) was also downregulated. Next, the localization of MHC class I molecules in these cells was assessed after they had been fixed and co-stained with anti-MHC class I and gB antibodies. MHC class I in infected cells was localized mainly within intracellular compartments, and colocalized with the envelope glycoprotein gB during the later stages of infection; however, MHC class I was mainly localized to the plasma membrane in mock-infected cells (Fig. 2c).

DISCUSSION

Here, we used mass spectrometry-based proteomics analysis to show that MHC class I molecules are incorporated into HHV-6 viral particles. Downregulation of MHC class I molecules in virus-infected cells is an important mechanism by which viruses evade immune surveillance (31–37). We showed that downregulation of MHC class I molecules occurs in T cells infected by HHV-6. MHC class I molecules are incorporated into viral particles and exosomes and then released into the extracellular environment, suggesting a possible strategy for escaping host immune responses. In addition, MHC class I molecules incorporated into virions and exosomes may assist viral entry. Further studies are needed to address this question.

We have previously reported that immature HHV-6 particles bud into TGN or TGN-derived vesicles (which are produced in HHV-6B-infected cells), that vesicles containing mature virions become MVBs, and that virions and exosomes are released into the extracellular environment via an exosomal secretary pathway (23). It is possible that MHC class I molecules are transported into the TGN-derived membranes from which the virions bud and then incorporated into virions within infected cells without being recycled (Fig. 3).

Within infected cells, MHC class I molecules colocalized with the gB protein in the cytoplasm indicating that, like viral glycoproteins, they are sorted into vesicles. The reduction in the total (both cell surface and

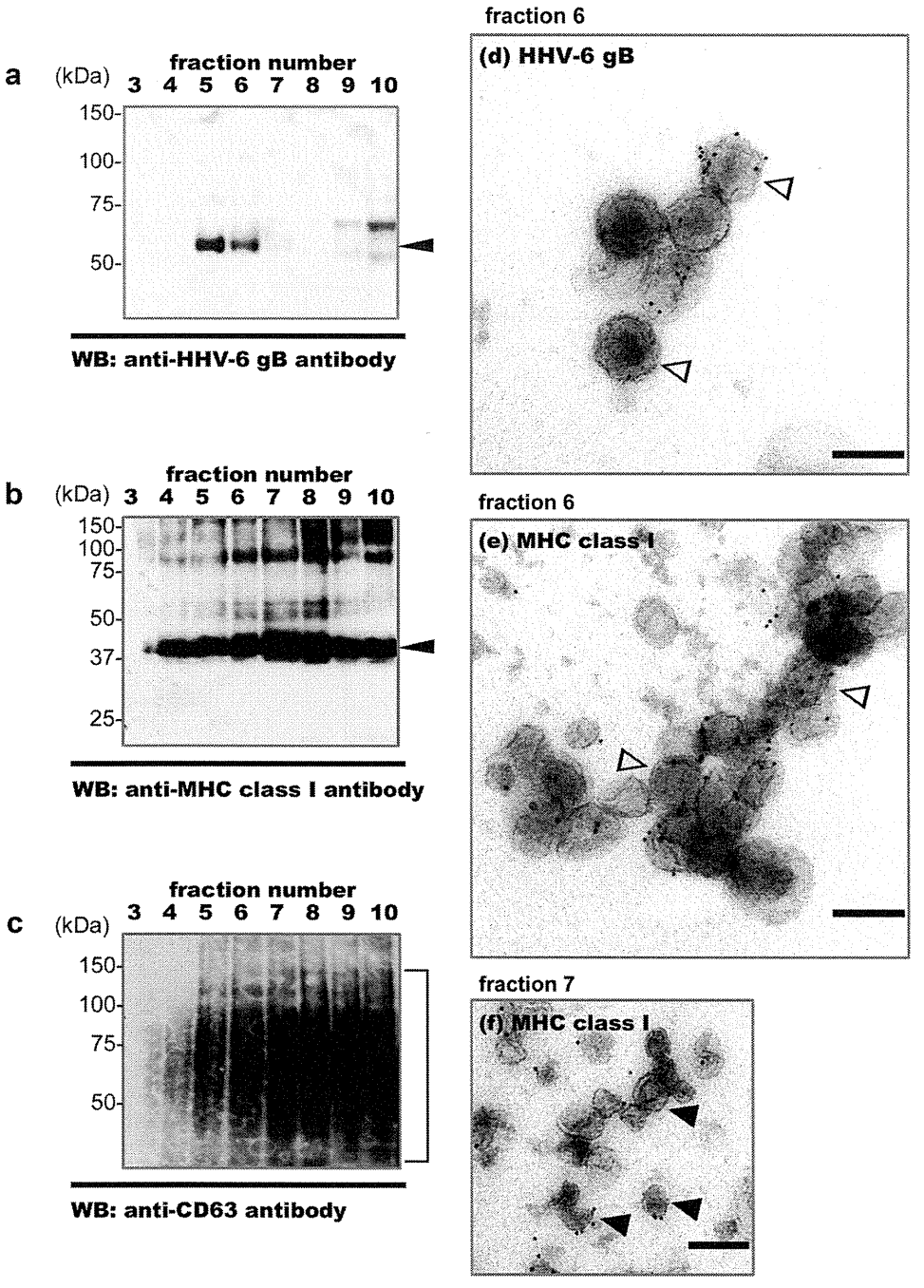

Fig. 1. MHC class I molecules are incorporated into virions and exosomes and released from HHV-6B-infected cells. Virions and exosomes were collected from the culture medium of HHV-6B-infected cells by sucrose density gradient centrifugation and examined by (a–c) western blotting and (d–f) electron microscopy. Western blots with (a) anti-gB rabbit, (b) anti-MHC class I (W6/32) or (c) anti-CD63 (CLB-gran/12, 435) antibodies are shown. The same amount of each protein fraction was added to each well of the gel. Immunogold labeling of (d) gB in fraction 6 and of (e,f) MHC class I in fractions 6 and 7. The fractions were collected from the bottom of tube. Hollow arrowheads, labeled virions; filled arrowheads, exosomes. Scale bars: 200 nm (d–f).

intracellular) expression of MHC class I in HHV-6-infected cells suggests that some of them may be transported to lysosomes and degraded, as this route is the same as that used to transport particles to MVBs.

Although several host proteins are usually expressed on the surfaces of uninfected cells, they are expressed in the same intracellular compartments as those in which viral particles incorporated. Newly formed compartments

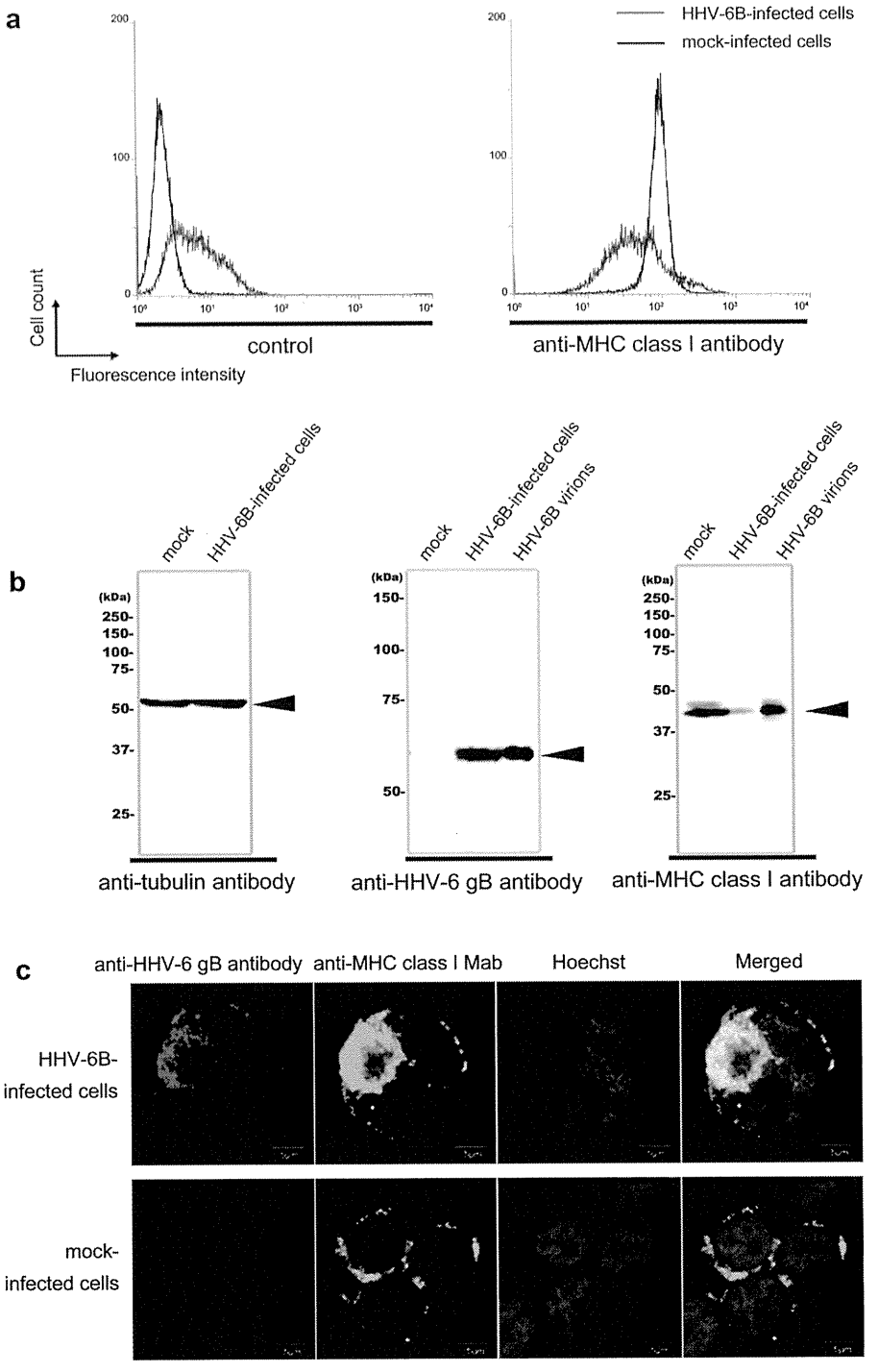

Fig. 2. Expression of MHC class I in HHV-6B-infected cells. (a) Expression of MHC class I on the surface of HHV-6B-infected cells is downregulated. HHV-6B-infected or mock-infected cells were harvested at 72 hr post-infection and fixed with 4% (w/v) paraformaldehyde. Fixed cells were stained with an anti-MHC class I antibody followed by staining with a secondary antibody prior to flow cytometric analysis. Control samples were incubated with the secondary antibody alone. Black histogram, mock-infected cells; blue histogram, HHV-6B- infected cells. (b) The total expression of MHC class I in HHV-6-infected cells was reduced. HHV-6B-infected or mock-infected cells were harvested at 72 hr post-infection and cell lysates prepared for western blotting. Purified HHV-6B virions were also used for western blotting. (c) MHC class I colocalizes with HHV-6B gB in intracellular compartments. HHV-6B-infected or mock-infected cells were harvested at 72 hr post-infection and fixed in cold acetone–methanol. Fixed cells were stained with antibodies against HHV-6 gB or MHC class I and with Hoechst33342. The stained cells were observed under a confocal microscope. The merged panels show the colocalized HHV-6 gB and MHC class I molecules. Single sections are shown. Scale bars: 5 micro meter.

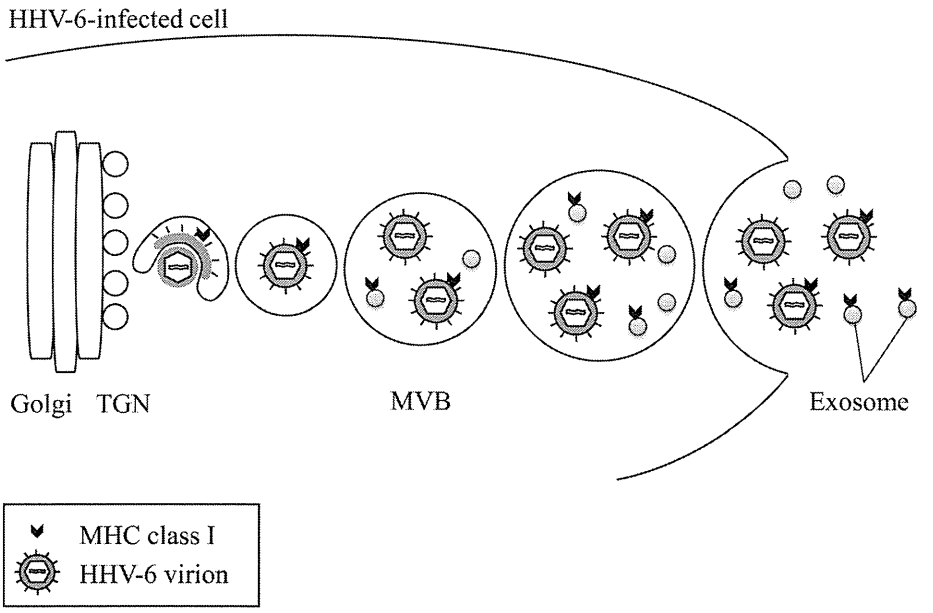

Fig. 3. Scematic representation of the fate of MHC class I molecules in HHV-6-infected cells. MHC class I molecules are transported to TGN- or post-TGN-derived vacuoles in HHV-6-infected cells and then incorporated into virions and intracellular small vesicles, which later become exosomes. Finally, MHC class I molecules are released from HHV-6-infected cells along with virions and exosomes.

within HHV-6-infected cells may show the combined characteristics of early and late endosomes. Recycling to early endosomes in HHV-6-infected cells may be modified or defective; therefore, several cellular proteins that use the same recycling system may be incorporated into virions and exosomes.

ACKNOWLEDGMENTS

We thank Dr. Kazushige Adachi (Minoh City Hospital) and Dr. Hideto Yamada (Department of Obstetrics and Gynecology, Kobe University Graduate School of Medicine) for providing the CBMCs. We also thank Ms. Eiko Moriishi (National Institute of Biomedical Innovation) for her technical support. This study was supported in part by a Grant-in-Aid for Scientific Research (B) and a Grant-in-Aid for Exploratory Research from the Japan Society for the Promotion of Science (JSPS).

DISCLOSURE

The authors declare that they have no competing interests.

REFERENCES

1. Roizmann B., Desrosiers R.C., Fleckenstein B., Lopez C., Minson A.C., Studdert M.J. (1992) The family Herpesviridae: an update. The Herpesvirus Study Group of the International Committee on Taxonomy of Viruses. *Arch Virol* **123**: 425–49.
2. Salahuddin S.Z., Ablashi D.V., Markham P.D., Josephs S.F., Sturzenegger S., Kaplan M., Halligan G., Biberfeld P., Wong-Staal F., Kramarsky B., Gallo R.C. (1986) Isolation of a new virus, HBLV, in patients with lymphoproliferative disorders. *Science* **234**: 596–601.
3. Aubin J.T., Collandre H., Candotti D., Ingrand D., Rouzioux C., Burgard M., Richard S., Huraux J.M., Agut H. (1991) Several groups among human herpesvirus 6 strains can be distinguished by Southern blotting and polymerase chain reaction. *J Clin Microbiol* **29**: 367–72.
4. Campadelli-Fiume G., Guerrini S., Liu X., Foa-Tomasi L. (1993) Monoclonal antibodies to glycoprotein B differentiate human herpesvirus 6 into two clusters, variants A and B. *J Gen Virol* **74**(Pt 10) 2257–62.
5. Wyatt L.S., Balachandran N., Frenkel N. (1990) Variations in the replication and antigenic properties of human herpesvirus 6 strains. *J Infect Dis* **162**: 852–7.
6. Yamanishi K., Okuno T., Shiraki K., Takahashi M., Kondo T., Asano Y., Kurata T. (1988) Identification of human herpesvirus-6 as a causal agent for exanthem subitum. *Lancet* **1**: 1065–7.
7. Okuno T., Takahashi K., Balachandra K., Shiraki K., Yamanishi K., Takahashi M., Baba K. (1989) Seroepidemiology of human herpesvirus 6 infection in normal children and adults. *J Clin Microbiol* **27**: 651–3.
8. Ahn K., Gruhler A., Galocha B., Jones T.R., Wiertz E.J., Ploegh H.L., Peterson P.A., Yang Y., Fruh K. (1997) The ER-luminal domain of the HCMV glycoprotein US6 inhibits peptide translocation by TAP. *Immunity* **6**: 613–21.
9. Hill A., Jugovic P., York I., Russ G., Bennink J., Yewdell J., Ploegh H., Johnson D. (1995) Herpes simplex virus turns off the TAP to evade host immunity. *Nature* **375**: 411–5.

10. Tomazin R., Van Schoot N.E., Goldsmith K., Jugovic P., Sempe P., Fruh K., Johnson D.C. (1998) Herpes simplex virus type 2 ICP47 inhibits human TAP but not mouse TAP. *J Virol* **72**: 2560–3.
11. Wills M.R., Ashiru O., Reeves M.B., Okecha G., Trowsdale J., Tomasec P., Wilkinson G.W., Sinclair J., Sissons J.G. (2005) Human cytomegalovirus encodes an MHC class I-like molecule (UL142) that functions to inhibit NK cell lysis. *J Immunol* **175**: 7457–65.
12. Jones T.R., Wiertz E.J., Sun L., Fish K.N., Nelson J.A., Ploegh H.L. (1996) Human cytomegalovirus US3 impairs transport and maturation of major histocompatibility complex class I heavy chains. *Proc Natl Acad Sci USA* **93**: 11,327–33.
13. Wiertz E.J., Jones T.R., Sun L., Bogyo M., Geuze H.J., Ploegh H.L. (1996) The human cytomegalovirus US11 gene product dislocates MHC class I heavy chains from the endoplasmic reticulum to the cytosol. *Cell* **84**: 769–79.
14. Ziegler H., Thale R., Lucin P., Muranyi W., Flohr T., Hengel H., Farrell H., Rawlinson W., Koszinowski U.H. (1997) A mouse cytomegalovirus glycoprotein retains MHC class I complexes in the ERGIC/cis-Golgi compartments. *Immunity* **6**: 57–66.
15. Coscoy L., Ganem D. (2000) Kaposi's sarcoma-associated herpesvirus encodes two proteins that block cell surface display of MHC class I chains by enhancing their endocytosis. *Proc Natl Acad Sci USA* **97**: 8051–6.
16. Hudson A.W., Howley P.M., Ploegh H.L. (2001) A human herpesvirus 7 glycoprotein, U21, diverts major histocompatibility complex class I molecules to lysosomes. *J Virol* **75**: 12347–58.
17. Ishido S., Wang C., Lee B.S., Cohen G.B., Jung J.U. (2000) Downregulation of major histocompatibility complex class I molecules by Kaposi's sarcoma-associated herpesvirus K3 and K5 proteins. *J Virol* **74**: 5300–9.
18. Reusch U., Muranyi W., Lucin P., Burgert H.G., Hengel H., Koszinowski U.H. (1999) A cytomegalovirus glycoprotein re-routes MHC class I complexes to lysosomes for degradation. *EMBO J* **18**: 1081–91.
19. Hirata Y., Kondo K., Yamanishi K. (2001) Human herpesvirus 6 downregulates major histocompatibility complex class I in dendritic cells. *J Med Virol* **65**: 576–83.
20. Glosson N.L., Hudson A.W. (2007) Human herpesvirus-6A and -6B encode viral immunoevasins that downregulate class I MHC molecules. *Virology* **365**: 125–35.
21. Mori Y., Yagi H., Shimamoto T., Isegawa Y., Sunagawa T., Inagi R., Kondo K., Tano Y., Yamanishi K. (1998) Analysis of human herpesvirus 6 U3 gene, which is a positional homolog of human cytomegalovirus UL 24 gene. *Virology* **249**: 129–39.
22. Mori Y., Akkapaiboon P., Yang X., Yamanishi K. (2003) The human herpesvirus 6 U100 gene product is the third component of the gH-gL glycoprotein complex on the viral envelope. *J Virol* **77**: 2452–8.
23. Mori Y., Koike M., Moriishi E., Kawabata A., Tang H., Oyaizu H., Uchiyama Y., Yamanishi K. (2008) Human herpesvirus-6 induces MVB formation, and virus egress occurs by an exosomal release pathway. *Traffic* **9**: 1728–42.
24. Okuno T., Shao H., Asada H., Shiraki K., Takahashi M., Yamanishi K. (1992) Analysis of human herpesvirus 6 glycoproteins recognized by monoclonal antibody OHV1. *J Gen Virol* **73**(Pt 2) 443–7.
25. Tang H., Kawabata A., Takemoto M., Yamanishi K., Mori Y. (2008) Human herpesvirus-6 infection induces the reorganization of membrane microdomains in target cells, which are required for virus entry. *Virology* **378**: 265–71.
26. Kawabata A., Tang H.M., Huang H.L., Yamanishi K., Mori Y. (2009) Human herpesvirus 6 envelope components enriched in lipid rafts: evidence for virion-associated lipid rafts. *Virology J* **6**: 127.
27. Yamada M., Mugnai G., Serada S., Yagi Y., Naka T., Sekiguchi K. (2013) Substrate-attached materials are enriched with tetraspanins and are analogous to the structures associated with rear-end retraction in migrating cells. *Cell Adh Migr* **7**: 304–14.
28. Akkapaiboon P., Mori Y., Sadaoka T., Yonemoto S., Yamanishi K. (2004) Intracellular processing of human herpesvirus 6 glycoproteins Q1 and Q2 into tetrameric complexes expressed on the viral envelope. *J Virol* **78**: 7969–83.
29. Mori Y., Akkapaiboon P., Yonemoto S., Koike M., Takemoto M., Sadaoka T., Sasamoto Y., Konishi S., Uchiyama Y., Yamanishi K. (2004) Discovery of a second form of tripartite complex containing gH-gL of human herpesvirus 6 and observations on CD46. *J Virol* **78**: 4609–16.
30. Raposo G., Nijman H.W., Stoorvogel W., Liejendekker R., Harding C.V., Melief C.J., Geuze H.J. (1996) B lymphocytes secrete antigen-presenting vesicles. *J Exp Med* **183**: 1161–72.
31. Elboim M., Grodzovski I., Djian E., Wolf D.G., Mandelboim O. (2013) HSV-2 specifically down regulates HLA-C expression to render HSV-2-infected DCs susceptible to NK cell killing. *PLoS Pathog* **9**: e1003226.
32. Kubota A., Kubota S., Farrell H.E., Davis-Poynter N., Takei F. (1999) Inhibition of NK cells by murine CMV-encoded class I MHC homologue m144. *Cell Immunol* **191**: 145–51.
33. Ma G., Feineis S., Osterrieder N., Van De Walle G.R. (2012) Identification and characterization of equine herpesvirus type 1 pUL56 and its role in virus-induced downregulation of major histocompatibility complex class I. *J Virol* **86**: 3554–63.
34. Neumann L., Kraas W., Uebel S., Jung G., Tampe R. (1997) The active domain of the herpes simplex virus protein IC P47: a potent inhibitor of the transporter associated with antigen processing. *J Mol Biol* **272**: 484–92.
35. Raafat N., Sadowski-Cron C., Mengus C., Heberer M., Spagnoli G.C., Zajac P. (2012) Preventing vaccinia virus class-I epitopes presentation by HSV-ICP47 enhances the immunogenicity of a TAP-independent cancer vaccine epitope. *Int J Cancer* **131**: E659–69.
36. Said A., Azab W., Damiani A., Osterrieder N. (2012) Equine herpesvirus type 4 UL56 and UL49.5 proteins downregulate cell surface major histocompatibility complex class I expression independently of each other. *J Virol* **86**: 8059–71.
37. Vasireddi M., Hilliard J. (2012) Herpes B virus, macacine herpesvirus 1, breaks simplex virus tradition via major histocompatibility complex class I expression in cells from human and macaque hosts. *J Virol* **86**(12) 503–11.

ARTHRITIS & RHEUMATOLOGY
Vol. 67, No. 2, February 2015, pp 498–507
DOI 10.1002/art.38953

Elevated Levels of Pentraxin 3 in Systemic Sclerosis

Associations With Vascular Manifestations and Defective Vasculogenesis

Yuichiro Shirai,[1] Yuka Okazaki,[2] Yumiko Inoue,[1] Yuichi Tamura,[1] Hidekata Yasuoka,[1] Tsutomu Takeuchi,[1] and Masataka Kuwana[2]

Objective. **To clarify the role of pentraxin 3 (PTX3), a multifunctional pattern recognition protein that can suppress fibroblast growth factor 2 (FGF-2), in systemic sclerosis (SSc)–related vasculopathy.**

Methods. **We assessed 171 SSc patients and 19 age- and sex-matched healthy control subjects. Circulating PTX3 and FGF-2 levels were measured by enzyme immunoassay, and CD34+CD133+CD309+ endothelial progenitor cells (EPCs) were counted by flow cytometry. Correlations between PTX3 and FGF-2 and the presence or future development of vascular manifestations, including digital ulcers and pulmonary arterial hypertension (PAH), were identified by univariate and multivariate analysis. The effect of PTX3 on EPC differentiation was evaluated in proangiogenic cultures of mouse bone marrow cells in combination with colony formation assay.**

Results. **Circulating PTX3 and FGF-2 levels were significantly higher in SSc patients than in healthy control subjects. PTX3 was elevated in SSc patients who had digital ulcers or PAH, while FGF-2 was reduced in SSc patients with PAH. Multivariate analysis identified elevated PTX3 as an independent parameter associated with the presence of digital ulcers and PAH, and PTX3 levels were a useful predictor of future occurrences of digital ulcers. Reduced FGF-2 was independently associated with the presence of PAH. EPC counts were significantly lower in patients with digital ulcers or PAH and correlated negatively with circulating PTX3 concentrations. Finally, PTX3 inhibited EPC differentiation in vitro.**

Conclusion. **In SSc patients, exposure to high concentrations of PTX3 may suppress EPC-mediated vasculogenesis and promote vascular manifestations such as digital ulcers and PAH.**

Systemic sclerosis (SSc) is a multisystem disease characterized by microvascular abnormalities and excessive fibrosis (1). It has been suggested that the pathogenic process of SSc is triggered by endothelial damage and the subsequent activation of immune cells and fibroblasts, resulting in excessive accumulation of extracellular matrix (2). Although several soluble mediators, including growth factors, cytokines, chemokines, and proangiogenic and antiangiogenic factors, are known to play critical roles in the pathogenesis of SSc, the mechanisms regulated by the interactions of these mediators are not clearly understood (2).

Pentraxin 3 (PTX3) is a pattern recognition protein belonging to the pentraxin superfamily (3). C-reactive protein (CRP), a short pentraxin, is primarily produced in the liver in response to interleukin-6 (IL-6). In contrast, PTX3 is produced locally at the inflammation site by macrophages, dendritic cells, endothelial cells (ECs), smooth muscle cells, and fibroblasts (4), and it is induced by Toll-like receptor agonists or proinflammatory cytokines such as IL-1β and tumor necrosis factor α, but not IL-6. Recently, several lines of evidence have shown that PTX3 has nonredundant roles in antimicrobial innate immunity, inflammation, extracellular matrix deposition, and neovascularization (4). Specifi-

Supported by the Japanese Ministry of Health, Labor, and Welfare (Research on Intractable Diseases grant).

[1]Yuichiro Shirai, MD, Yumiko Inoue, MD, Yuichi Tamura, MD, PhD, Hidekata Yasuoka, MD, PhD, Tsutomu Takeuchi, MD, PhD: Keio University School of Medicine, Tokyo, Japan; [2]Yuka Okazaki, BS, Masataka Kuwana, MD, PhD: Keio University School of Medicine and Nippon Medical School Graduate School of Medicine, Tokyo, Japan.

Address correspondence to Masataka Kuwana, MD, PhD, Department of Allergy and Rheumatology, Nippon Medical School Graduate School of Medicine, 1-1-5 Sendagi, Bunkyo-ku, Tokyo 113-8603, Japan. E-mail: kuwanam@nms.ac.jp.

Submitted for publication June 29, 2014; accepted in revised form November 6, 2014.

cally, it binds to apoptotic cells and selected pathogens, and it activates and modulates the classical complement pathway by binding to C1q. PTX3 is also a component of the extracellular matrix and contributes to fibrosis in this role. Finally, PTX3 acts as an antiangiogenic factor by binding to fibroblast growth factor 2 (FGF-2) with high affinity and specificity and inhibiting FGF-2–dependent EC proliferation and neovascularization (5).

The pleiotropic effects of PTX3 on inflammation and fibrosis, along with its inhibition of neovascularization, suggest that it is an intriguing candidate as a mediator in the pathogenesis of SSc. In fact, circulating PTX3 levels are elevated in SSc patients (6), and PTX3 is up-regulated in ECs and fibroblasts in affected skin (6–8). In addition, cultured fibroblasts derived from SSc skin constitutively expressed PTX3 in the absence of agonistic stimulation (6,7). The silencing of PTX3 gene expression by small interfering RNA restored the impaired ability of cultured SSc microvascular ECs to form capillary-like tubes and promote vascularization (9). These findings suggest that PTX3, constitutively produced at the affected site, is involved in the pathogenesis of SSc. To test this hypothesis, we examined the roles of PTX3 in SSc pathogenesis by evaluating potential correlations between SSc manifestations and circulating levels of PTX3 and FGF-2, and by investigating the mechanisms underlying these correlations.

PATIENTS AND METHODS

Patients and controls. This study included 171 consecutive patients with SSc (15 men and 156 women) who visited an SSc clinic at Keio University Hospital between 2007 and 2013. All patients met the American College of Rheumatology (ACR)/European League Against Rheumatism 2013 classification criteria for SSc (10), and 137 patients (80%) also met the 1980 ACR preliminary classification criteria (11). Peripheral blood samples were collected from all patients when they entered the study and from a subset of patients 2 years later. Peripheral blood was also collected from 19 healthy control subjects matched for age and sex (4 men and 15 women). The heparinized blood was immediately separated into platelet-poor plasma and mononuclear cells, which were used to count endothelial progenitor cells (EPCs). Serum and plasma samples were stored at −80°C until use. We obtained informed written consent from all subjects prior to collecting samples in accord with the tenets of the Declaration of Helsinki, and all study protocols were approved by the Institutional Review Board of Keio University School of Medicine.

Clinical assessment. A complete medical history, physical examination, and laboratory evaluation were performed for each patient at the time of enrollment, and limited evaluations were conducted at each followup visit. Patients were carefully monitored for new-onset digital ulcers and pulmonary arterial hypertension (PAH) through December 2013. We collected the following data for each patient: age, sex, disease subset, disease duration from first appearance of non–Raynaud's phenomenon symptoms, disease duration from first appearance of Raynaud's phenomenon, modified Rodnan skin thickness score (MRSS) (12), and SSc-related organ involvement, including digital ulcers, interstitial lung disease (ILD), PAH, and any heart, upper gastrointestinal (GI), lower GI, or renal involvement. We also recorded treatment profiles and any risk factors for atherosclerosis, including hypertension, dyslipidemia, diabetes mellitus, and whether the patient was a current or former smoker. SSc was classified as diffuse cutaneous SSc (dcSSc) or limited cutaneous SSc (lcSSc) according to the system described by Medsger (13).

SSc-related organ involvement was defined as described previously (14) with modifications. A digital ulcer was defined as a loss of both epidermis and dermis in an area at least 2 mm in diameter located at the volar surface of the digit distal to the proximal interphalangeal digital crease (15). ILD was defined as bilateral reticulations, ground-glass opacity, and/or honeycombing seen on chest radiograph or high-resolution computed tomographic scan of the lungs. PAH was defined as a mean pulmonary arterial pressure of ≥25 mm Hg and pulmonary vascular resistance of >3 Wood units, measured by right-sided heart catheterization with the patient at rest, after exclusion of pulmonary hypertension due to left-sided heart disease (an end-expiratory pulmonary artery wedge pressure of >15 mm Hg), advanced ILD (forced vital capacity <70% of predicted), or chronic thromboembolism (16). Heart involvement was defined as clinical evidence of symptomatic pericardial effusion, congestive heart failure, or arrhythmia considered to be due to SSc and requiring treatment. Upper GI involvement was defined as distal esophageal hypomotility demonstrated by cine-esophagram or manometry. Lower GI involvement was defined as radiologic evidence of wide-mouthed colonic sacculations or small intestinal dysmotility, malabsorption, or small bowel bacterial overgrowth requiring administration of antibiotics. Renal involvement was defined as acute or subacute development of renal insufficiency often, but not always, associated with accelerated hypertension and/or microangiopathic hemolytic anemia. Extensive ILD was defined as described by Goh et al (17).

SSc-related autoantibodies. The following antibodies were identified by indirect immunofluorescence using commercially prepared slides of monolayer HEp-2 cells (MBL) and immunoprecipitation assays: anticentromere, anti–topoisomerase I, anti–RNA polymerase III, anti–U1 RNP, anti–U3 RNP, anti–U11/U12 RNP, anti-Th/To, anti–PM-Scl, anti-Ku, and anti-RuvBL1/2 (18).

Measurement of PTX3 and FGF-2 in the circulation. Concentrations of PTX3 in plasma and FGF-2 in serum were measured in duplicate using enzyme immunoassay kits according to the manufacturers' instructions (Perseus Proteomics and R&D Systems, respectively). The lower limits of detection for PTX3 and FGF-2 were 0.1 ng/ml and 3 pg/ml, respectively. The coefficients of variation of 2 values ranged from 0 to 0.25. In some analyses, the ratio of PTX3 (ng/ml) to FGF-2 (ng/ml) was used as an indicator of the anti/proangiogenic activity of FGF-2 signaling.

Quantification of EPCs. The absolute number of CD34+CD133+CD309+ EPCs in peripheral blood was deter-

mined as described previously (19) and is shown as the number per 1 ml of peripheral blood, determined using FlowCount fluorospheres (Beckman Coulter) as an internal calibrator.

EPC colony formation assay. The ability of mouse bone marrow stem cells to differentiate into EPCs in the presence of a series of proangiogenic factors, including FGF-2, was assessed by colony formation assay as described previously (20). Briefly, bone marrow mononuclear cells were isolated from the thigh bones of 10–12-week-old male C57BL/6J mice. The cells were suspended in Dulbecco's modified Eagle's medium containing 10% fetal bovine serum (Sigma-Aldrich) and seeded on Pronectin (Sigma-Aldrich)–coated 60-mm culture dishes. After 24 hours, nonadherent mononuclear cells were collected and cultured on Pronectin-coated UpCell 6-well plates with EGM-2 supplemented with SingleQuots (Lonza), which contains 2% fetal bovine serum and other components (hydrocortisone, insulin-like growth factor 1 [IGF-1], epidermal growth factor [EGF], vascular endothelial growth factor [VEGF], FGF-2, ascorbic acid, and heparin) with no information available on individual concentrations, either with or without recombinant mouse PTX3 (5 or 20 n*M*; R&D Systems).

After 6 days, adherent cells were subjected in duplicate to a colony assay that can be used to evaluate colony-forming unit (CFU)–EC colonies and CFU–granulocyte–erythrocyte–macrophage–megakaryocyte (GEMM) colonies simultaneously. The culture medium used was MethoCult (StemCell Technologies) with stem cell factor (100 ng/ml), IL-3 (20 ng/ml), IGF-1 (50 ng/ml), EGF (50 ng/ml), VEGF (50 ng/ml), FGF-2 (50 ng/ml) (all from R&D Systems), insulin (10 μg/ml; PromoCell), and transferrin (200 μg/ml; Sigma-Aldrich). After 14 days, CFU-EC and CFU-GEMM colonies were individually counted using a microscope at 20× magnification. Results are shown as the mean of the 2 measurements.

Statistical analysis. All continuous variables are shown as the mean ± SD. Paired and unpaired comparisons of continuous variables were made using Wilcoxon tests or Mann-Whitney U tests, respectively. Categorical variables were compared using Fisher's exact test or a chi-square test when appropriate. The correlation coefficient (r) was calculated using Pearson's regression model. Variables that best explained the risk of digital ulcers and PAH were identified by multivariate logistic regression analysis combining clinical parameters (sex, age at onset and at entry into the study, disease duration from first appearance of non–Raynaud's phenomenon symptoms and from first appearance of Raynaud's phenomenon, disease subset, Raynaud's phenomenon, individual organ involvement, and previous history of digital ulcers), autoantibodies, corticosteroid use, and circulating levels of PTX3 and FGF-2. Results are presented as odds ratios (ORs) with 95% confidence intervals (95% CIs). The Cox proportional hazards regression model was used to determine factors associated with an increased risk of the future development of digital ulcers. Results are presented as hazard ratios (HRs) with 95% CIs. The cutoff value that best discriminated 2 groups was determined by receiver operating characteristic (ROC) curve analysis. Survival analysis was performed using the Kaplan-Meier method, and survival was compared between 2 groups by log rank test. All statistical analyses were performed using SPSS 19.0 statistical software.

RESULTS

Levels of circulating PTX3 and FGF-2 in SSc patients. Demographic and clinical characteristics were recorded and blood samples were obtained from each of the 171 SSc patients as they entered the study (Table 1). Our cohort consisted mainly of patients with lcSSc (74%). The mean ± SD disease durations from the first appearance of non–Raynaud's phenomenon symptoms and from the first appearance of Raynaud's phenomenon were 9.5 ± 7.2 years and 14.0 ± 9.9 years, respectively. Figure 1 shows that in comparison to healthy control subjects, SSc patients had significantly higher

Table 1. Demographic and clinical characteristics of the 171 SSc patients at the time of enrollment*

Female	156 (91)
Age at SSc onset, mean ± SD years	51 ± 14
Age when enrolled in study, mean ± SD years	60 ± 14
Disease duration from first appearance of non–Raynaud's phenomenon symptoms, mean ± SD years	9.5 ± 7.2
Disease duration from first appearance of Raynaud's phenomenon, mean ± SD years	14.0 ± 9.9
Diffuse cutaneous SSc	44 (26)
Modified Rodnan skin thickness score, mean ± SD	6.1 ± 7.5
Raynaud's phenomenon	165 (96)
Previous history of digital ulcer	16 (9)
Organ involvement	
Digital ulcer	17 (10)
Interstitial lung disease	83 (49)
Interstitial lung disease, extensive stage	29 (17)
Pulmonary arterial hypertension	21 (12)
Heart involvement	11 (6)
Upper gastrointestinal involvement	92 (54)
Lower gastrointestinal involvement	8 (5)
Renal involvement	2 (1)
Autoantibodies	
Anticentromere	69 (40)
Anti–topoisomerase I	46 (27)
Anti–U1 RNP	29 (17)
Anti-Th/To	8 (5)
Anti–RNA polymerase III	7 (4)
Anti–U3 RNP	2 (1)
Anti-Ku	1 (1)
C-reactive protein, mean ± SD mg/dl	0.25 ± 0.53
Treatment	
Corticosteroids (≤10 mg/day prednisolone equivalent)	23 (13)
Immunosuppressants	9 (5)
Phosphodiesterase 5 inhibitors	12 (7)
Endothelin receptor antagonists	8 (5)
Parenteral prostanoids	3 (2)
Risk factors for atherosclerosis	
Hypertension	15 (9)
Dyslipidemia	10 (6)
Diabetes mellitus	3 (2)
Current or former smoker	1 (1)

* Except where indicated otherwise, values are the number (%). SSc = systemic sclerosis.

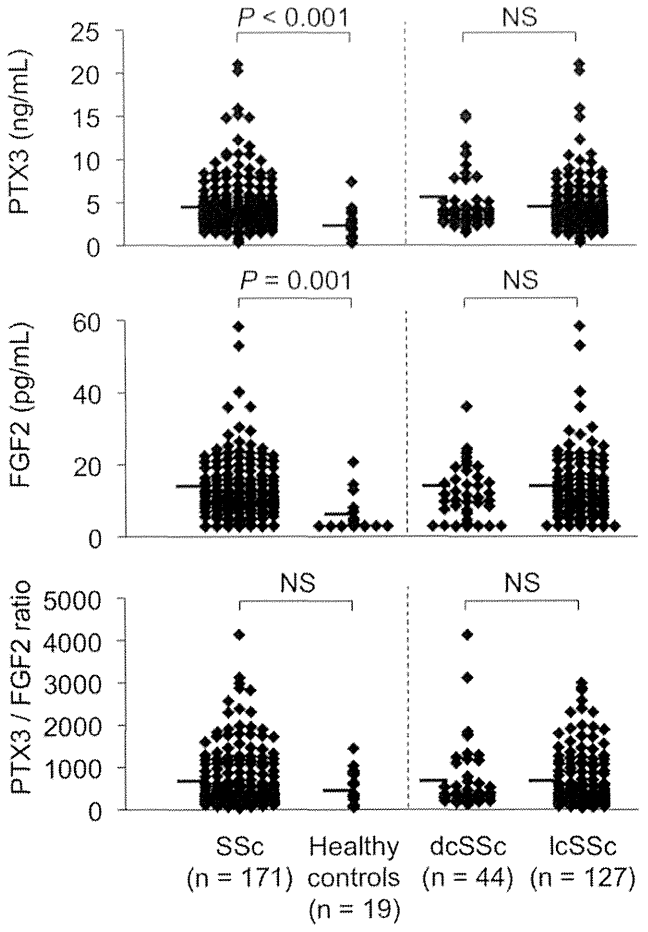

Figure 1. Levels of circulating pentraxin 3 (PTX3) and fibroblast growth factor 2 (FGF-2) and the PTX3:FGF-2 ratio in patients with systemic sclerosis (SSc) and in healthy control subjects. SSc patients were classified as having diffuse cutaneous SSc (dcSSc) or limited cutaneous SSc (lcSSc). Symbols represent individual subjects; bars show the mean. *P* values were determined by Mann-Whitney U test. NS = not significant.

levels of circulating PTX3 (mean ± SD 4.8 ± 3.3 ng/ml versus 2.4 ± 1.7 ng/ml) and FGF-2 (12.0 ± 9.4 pg/ml versus 5.8 ± 5.0 pg/ml). There were no differences in PTX3 or FGF-2 levels between SSc patients with dcSSc and those with lcSSc (Figure 1). The PTX3:FGF-2 ratio, which we used as an indicator of the relative anti/proangiogenic activity of FGF signaling, was not different between SSc patients and healthy controls. We did not find correlations between PTX3, FGF-2, and CRP levels in patients with SSc ($r < 0.1$ for all comparisons).

Association of organ involvement with circulating levels of PTX3 and FGF-2. PTX3 and FGF-2 levels were compared between SSc patients grouped by the presence or absence of specific organ involvement (further information is available at http://www.nms-rheum.jp). Statistically significant differences were detected when patients were divided by the presence or absence of digital ulcers or PAH (Figure 2). PTX3 was significantly elevated in patients with digital ulcers compared to those without digital ulcers, while there was no difference in FGF-2 concentrations. The presence of PAH, like the presence of digital ulcers, was associated with increased PTX3. However, in contrast to the similarity in FGF-2 levels between patients with and those

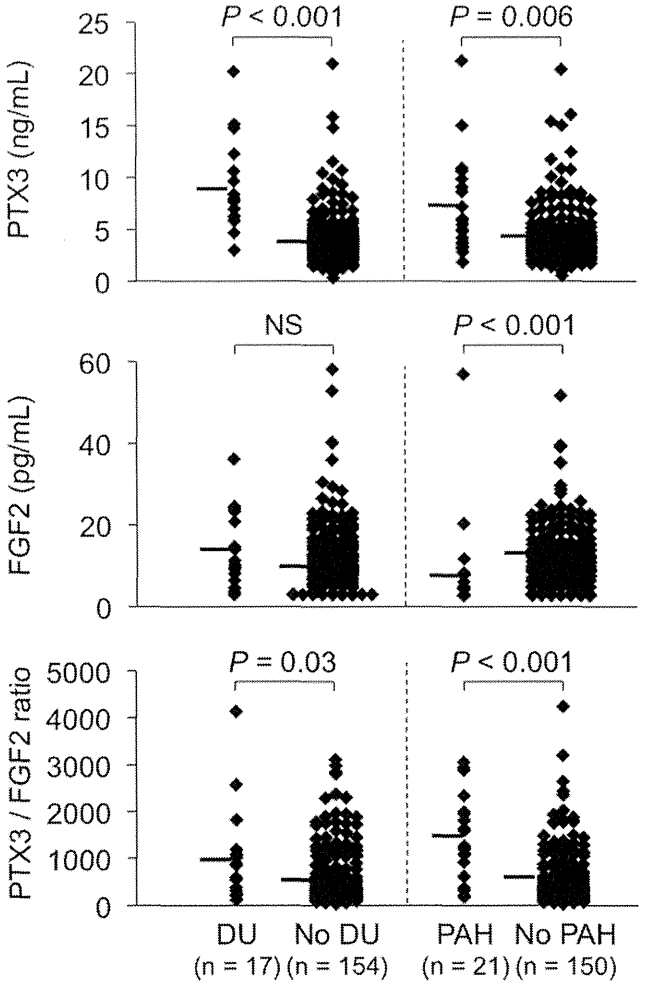

Figure 2. Levels of circulating PTX3 and FGF-2 and the PTX3:FGF-2 ratio in SSc patients grouped by the presence or absence of digital ulcers (DU) or pulmonary arterial hypertension (PAH). Symbols represent individual patients; bars show the mean. *P* values were determined by Mann-Whitney U test. See Figure 1 for other definitions.

without digital ulcers, levels of FGF-2 were decreased among patients with PAH compared to those without PAH (Figure 2). The mean ± SD FGF-2 level in SSc patients with PAH (8.1 ± 12.3 pg/ml) was comparable to that in healthy controls ($P = 0.8$). The PTX3:FGF-2 ratio was significantly higher in patients with digital ulcers or PAH than in those without, suggesting that FGF-2 signaling was suppressed. When we assessed potential associations of PTX3 and FGF-2 levels with risk factors for atherosclerosis and with specific treatments, PTX3 levels were found to be significantly higher in SSc patients receiving corticosteroids than in those not receiving them ($P = 0.02$).

As the behavior of FGF-2 appeared to change in association with digital ulcers or PAH, we divided SSc patients into 4 groups based on the presence or absence of digital ulcers and the presence or absence of PAH, and we evaluated the distribution of PTX3 and FGF-2 levels in each group (Figure 3). When PTX3 and FGF-2 levels were divided as high or low relative to the mean (3.88 ng/ml for PTX3 and 9.82 pg/ml for FGF-2), differences in patient distribution in the groups became apparent. All but 1 patient with digital ulcers was included in the high-PTX3 group, independent of the presence or absence of PAH, and the frequency of high PTX3 was significantly greater in patients with digital ulcers than in those without digital ulcers (94% versus 45%; $P < 0.001$). On the other hand, patients with PAH were more frequently included in the low–FGF-2 group than were those without PAH (86% versus 45%; $P < 0.001$). Thus, it is likely that different PTX3 and FGF-2 profiles regulate the development of digital ulcers and PAH. However, the PTX3:FGF-2 ratio was elevated both in patients with digital ulcers and in patients with PAH (Figure 2), indicating the presence of common antiangiogenic properties.

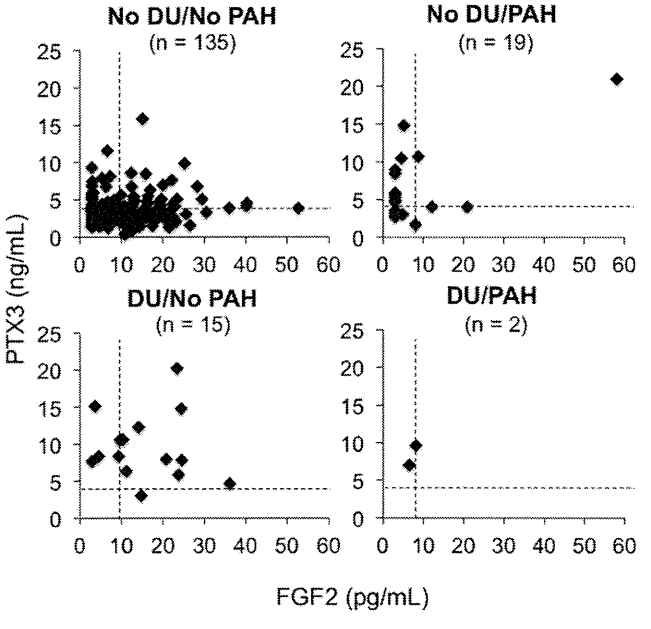

Figure 3. Distribution of PTX3 and FGF-2 levels in 4 groups of SSc patients stratified by the presence or absence of digital ulcers (DU) and pulmonary arterial hypertension (PAH). Dashed lines indicate mean PTX3 and FGF-2 levels in SSc patients (3.88 ng/ml and 9.82 pg/ml, respectively). Symbols represent individual patients. See Figure 1 for other definitions.

PTX3 and FGF-2 as independent parameters associated with digital ulcers or PAH. Using multivariate analysis, we further determined whether circulating PTX3 and FGF-2 levels were independently associated with the presence of digital ulcers or PAH (further information is available at http://www.nms-rheum.jp). Univariate analyses identified disease duration from the first appearance of non–Raynaud's phenomenon symptoms, dcSSc, a previous history of digital ulcers, upper GI involvement, and anti–topoisomerase I antibody as parameters potentially associated with the presence of digital ulcers ($P < 0.1$). Multivariate logistic regression analysis of these parameters along with PTX3 and FGF-2 levels identified the following as independent parameters positively associated with digital ulcers: PTX3 (OR 1.50 [95% CI 1.22–1.85], $P < 0.001$), anti–topoisomerase I antibody (OR 8.01 [95% CI 1.13–57.1], $P = 0.04$), and a previous history of digital ulcers (OR 61.7 [95% CI 7.09–537], $P < 0.001$).

To identify independent parameters associated with PAH, we conducted multivariate analysis with 5 variables: the absence of anti–topoisomerase I antibody, which was selected by univariate analysis; disease duration from the first appearance of Raynaud's phenomenon and lcSSc, which were previously reported to be associated with PAH (21); and PTX3 and FGF-2 (further information is available at http://www.nms-rheum.jp). PTX3 was the sole parameter positively associated with PAH (OR 1.23 [95% CI 1.08–1.40], $P = 0.002$), while FGF-2 was identified as an independent parameter negatively associated with PAH (OR 0.92 [95% CI 0.85–0.99], $P = 0.02$). When these analyses were repeated using the PTX3:FGF-2 ratio instead of PTX3 and FGF-2 levels, the PTX3:FGF-2 ratio was selected as an independent parameter associated with digital ulcers (OR 1.001 [95% CI 1.000–1.002], $P = 0.04$) and PAH (OR 1.001 [95% CI 1.001–1.002], $P < 0.001$).

Predictors of a new occurrence of digital ulcers. Of 171 patients at the initial evaluation, 148 had never

developed digital ulcers. These patients were prospectively followed up for a mean ± SD of 3.4 ± 2.5 years, and 18 (12%) developed digital ulcers for the first time during the followup period. ROC curve analysis was used to determine whether circulating levels of PTX3 and FGF-2, as well as the PTX3:FGF-2 ratio, were predictive of new digital ulcer development (Figure 4A). PTX3 levels and the PTX3:FGF-2 ratio were found to be useful in predicting the future onset of digital ulcers, but FGF-2 levels were not. The cutoff values that best discriminated a risk of future digital ulcer development were 4.3 ng/ml for PTX3 and 344 for the PTX3:FGF-2 ratio. When SSc patients were divided by high or low PTX3 levels relative to the cutoff values, the cumulative occurrence rate of new digital ulcers changed significantly (Figure 4B). We were unable to conduct a similar analysis of PAH predictors because only 1 patient developed PAH during the followup period.

Using the Cox proportional hazards regression model, we further assessed whether the circulating PTX3 level was an independent parameter predicting the future development of digital ulcers (further information is available at http://www.nms-rheum.jp). In this analysis, the time origin was the time of enrollment. The variables included were dcSSc and anti–topoisomerase I antibody, which were selected by univariate analysis ($P < 0.1$); disease duration from the first appearance of non–Raynaud's phenomenon symptoms, which was previously shown to be associated with digital ulcers (22,23); and PTX3 and FGF-2. This identified PTX3 as the sole independent predictor for the new development of digital ulcers (HR 1.25 [95% CI 1.09–1.42], $P = 0.001$). When the analysis was repeated using the PTX3:FGF-2 ratio instead of PTX3 and FGF-2, the PTX3:FGF-2 ratio was selected as the sole predictor for the future development of digital ulcers (HR 1.001 [95% CI 1.000–1.001], $P = 0.003$).

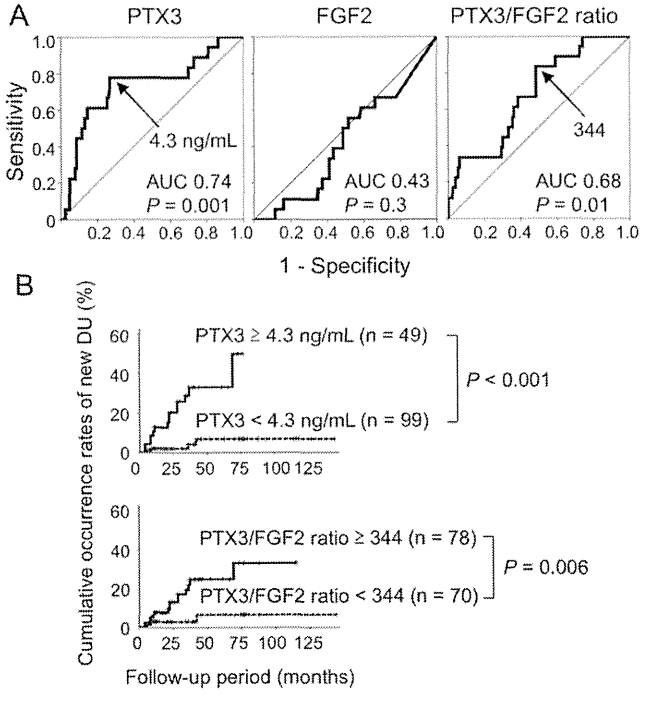

Figure 4. Predictors for new digital ulcers (DU) in 148 SSc patients who had never developed digital ulcers. **A,** Receiver operating characteristic curve analysis evaluating optimal cutoff values of PTX3 and FGF-2 levels and the PTX3:FGF-2 ratio for predicting new occurrences of digital ulcers. AUC = area under the curve. **B,** Kaplan-Meier analysis to evaluate cumulative occurrence rates of new digital ulcers in SSc patients stratified by PTX3 levels and the PTX3:FGF-2 ratio. *P* values were determined by log rank test. See Figure 1 for other definitions.

Changes in PTX3 and FGF-2 levels after an interval of 2 years. Followup blood samples obtained 2 years after the initial evaluation were available for 37 SSc patients, 9 of whom developed digital ulcers during this period. The levels of circulating PTX3 and FGF-2 were fairly stable between study enrollment and 2 years later, regardless of whether there was any new onset of digital ulcers (4.7 ± 3.3 ng/ml versus 4.4 ± 3.2 ng/ml and 10.7 ± 10.4 pg/ml versus 10.9 ± 7.1 pg/ml, respectively). Taken together, these results suggest that elevated PTX3 levels and PTX3:FGF-2 ratios are useful biomarkers to predict the future development of digital ulcers in SSc patients, and that high, persistent concentrations of PTX3 in the circulation may lead to the occurrence of digital ulcers.

Correlations between PTX3 and EPCs in the circulation. It was recently reported that the number of circulating EPCs is inversely correlated with the presence of digital ulcers, and that a low EPC count in SSc patients is a risk factor for developing digital ulcers (24,25). Thus, we investigated the potential correlation between circulating PTX3 levels and EPC counts. Circulating EPC counts obtained at the same time as PTX3 and FGF-2 levels were available for 70 patients. EPC counts were significantly lower in patients with digital ulcers than in those without digital ulcers and significantly lower in patients with PAH than in those without PAH (Figure 5A). EPC counts were negatively correlated with circulating PTX3 levels and PTX3:FGF-2 ratios, but there was no correlation with FGF-2 levels (Figure 5B). These findings demonstrated an association between reduced EPC counts and high concentrations of